Instrumented Footwear and Machine Learning for Gait Analysis and Training

Jesus Antonio Prado de la Mora

Submitted in partial fulfillment of the
requirements for the degree of
Doctor of Philosophy
under the Executive Committee
of the Graduate School of Arts and Sciences

COLUMBIA UNIVERSITY

2021

Abstract

Instrumented Footwear and Machine Learning for Gait Analysis and Training

Jesus Antonio Prado de la Mora

Gait analysis allows clinicians and researchers to quantitatively characterize the kinematics and kinetics of human movement. Devices that quantify gait can be either portable, such as instrumented shoes, or non-portable, such as motion capture systems and instrumented walkways. There is a tradeoff between these two classes of systems in terms of portability and accuracy. However, recent computer advances allow for the collection of meaningful data outside of the clinical setting. In this work, we present the DeepSole system combined with the different neural network models. This system is a fully capable to characterize the gait of the individuals and provide vibratory feedback to the wearer. Thanks to the flexible construction and its wireless capabilities, it can be comfortably worn by wide arrange of people, both able-bodied and people with pathologies that affect their gait. It can be used for characterization, training, and as an abstract sensor to measure human gait in real-time.

Three neural network models were designed and implemented to map the sensors embedded in the DeepSole system to gait characteristics and events. The first one is a recurrent neural network that classifies the gait into the correct gait phase of the wearer. This model was validated with data from healthy young adults and children with Cerebral Palsy. Furthermore, this model was implemented in real-time to provide vibratory feedback to healthy young adults to create temporal asymmetry on the dominant side during regular walking. During the experiment,

the subjects who walked had an increased stance time on both sides, but the dominant side was affected more.

The second model is encoder-decoder recurrent neural network that maps the sensors into current gait cycle percentage. This model is useful to provide continuous feedback that is synchronized to the gait. This model was implemented in real-time to provide vibratory feedback to six muscle groups used during regular walking. The effects of the vibration were analyzed. It was found that depending on the feedback, the subjects changed their spatial and temporal gait parameters.

The third model uses all the sensors in the instrumented footwear to identify a motor phenomenon called freezing of gait in patients with Parkinson's Disease. This phenomenon is characterized by transient periods, usually lasting for several seconds, in which attempted ambulation is halted. The model has better performance than the state-of-the-art and does not require any pre-processing.

The DeepSole system when used in conjunction with the presented models is able to characterize and provide feedback in a wide range of scenarios. The system is portable, comfortable, and can accommodate a wide range of populations who can benefit from this wearable technology.

Table of Contents

List of Figures

List of Tables

Acknowledgments

All my life I have been curious, always intrigued about how things work and asking questions. The desire to design and invent has driven me throughout the years, and this dissertation is the result of that ambition. While I am presenting my works here, it has been accomplished with the guidance, motivation, discussions, and support from others.

I would like to thank my advisor, Dr. Sunil Agrawal for guiding my research. I appreciate the advice given throughout the years to define the scope of my research, making it impactful, and teaching me to ask valuable scientific questions. The support given throughout the stages of my doctoral work has inspired me to pursue research that not only advances science, but also has a positive impact on the lives of others.

I would also like to thank my committee members, Dr. Matei Ciocarlie, Dr. Andy Gordon, Dr. Joel Stein, and Dr. Anil Lalwani for reviewing my research work and providing me with constructive feedback and valuable insight that improved my work. These, along with the insights provided by my clinical collaborators, Dr. Nora Vanegas-Arroyave and Dr. Kimberly Kwei, motivated my work and enhanced its innovation and impact within the rehabilitation field. I would also like to express my gratitude for everyone who participated in my studies; hearing their perspectives often motivated the next steps for my work. Without the guidance from all those who assisted me within the rehabilitation field, my work would not have reached its full potential, so I thank you.

A special thanks to all my labmates, from who I learned the most over these years. Not only did they provide me with knowledge and different perspectives, but they have created a fun environment where I can clear my mind when faced with difficult problems. To Dr. Haohan Zhang, for showing me that working on difficult scientific questions can be fun and rewarding. To Dr.

Moiz Khan, for helping me expand the scope of my research by showing me other applications that my work could have. To Dr. Dario Martelli, for teaching me to consider the behavioral aspects of my work, rather than solely focusing on the devices I designed. To Biing-Chwen Chang, for your insights about biomechanics and the discussions about extracting meaning from data. To Danielle Stramel, for pushing me to be proud of my work, reviewing my writing, and improving my vocabulary by doing daily crosswords. To Tatiana Luna, for always having conversations with me during the day, either for work or for entertainment. I would also like to extend my thanks to all the undergraduate and graduate students that have helped me with my research over the years.

This milestone would not have been possible without the support and love from all my family. I would like to thank my parents, Antonio and Silvia Prado, for always supporting me and teaching me to follow my passions. To my sisters, Litza and Viridiana Prado for encouraging to pursue my dreams even if they are far from home. To my nephews and nieces to always asking questions and having fun. To my grandmother Clelia Salazar, for her wisdom, love, encouragement throughout the years. To my wife, Mariana Basilio, for supporting me through the years, pushing me forward and inspiring me to follow my dreams. My family has been my motivation, inspiration, and drive to pursue my doctoral degree, without them I would not have been successful.

Introduction

The presented work shows the design and validation of an instrumented footwear system called DeepSole System. This wearable system can be used for gait analysis and training. Three main aims have been realized and presented.

The first aim is the design of an instrumented footwear that is comfortable and unobtrusive to the wearer. This is described in detailed in Chapter 1. Three main parts of the system are described: the insole module, the electronics modules, and the data recording and transmission. This system can be used both for gait analysis and gait training.

The second aim is to create algorithms that enhance the performance of the instrumented footwear. These algorithms are explained in Chapters 2, 3, and 4.

Chapter 2 describes a neural network model used for segmentation of the gait into strides and gait phases. This model was tested with young adults and in children with cerebral palsy. The study presented shows that the model is capable of segmenting and classifying the phase of the gait for both populations.

Chapter 3 expands on gait analysis by implementing a neural network model that can predict the current gait cycle percentage. To understand the best architecture for the neural network model, different models were tested with a dataset collected form healthy young adults. With this process, an architecture was found that is capable of continuously predicting the current gait cycle percentage at a continuous frequency of 50 Hz. This model uses the data from the instrumented footwear without any data preprocessing or human intervention.

Chapter 4 expands the gait characterization and uses the classification properties of the neural networks to identify a motor phenomenon in people with Parkinson's Disease called

Freezing of Gait. To achieve this, a dataset was collected from people who presented this phenomenon. The participants were asked to walk for six minutes and the session was recorded by the DeepSole system and a video camera. A clinical expert provided a detailed analysis of the video by identifying the freezing of gait events at a resolution of 1 seconds. This data was used to train a neural network model capable of identifying the events from the sensors embedded in the DeepSole System.

Finally, the third aim is to test the footwear and algorithms in real-time to provide gait training dependent on the gait of the individual. These experiments are described in Chapters 5 and 6.

Chapter 5 shows an experiment that utilizes the neural network model presented in Chapter 2. The model is used to identify the stance phase in real-time and provide vibratory feedback on the dominant foot of the subject. The goal of the feedback is to evaluate the effect of vibratory feedback to create temporal asymmetry in the gait of the subjects. This experiment shows that unilateral vibratory feedback can be used to create temporal asymmetry in the gait of the subjects. Although, given that walking is a bilateral activity, changing one side influences the other side as well.

Chapter 6 uses the neural network presented in Chapter 3 and expands the DeepSole system to provided muscle vibration, timed to the gait cycle prediction. In this experiment, healthy young adults walked with two different types of vibration. The six vibration motors were mounted on different muscle groups on the legs of the subjects. The vibration motors were mounted at the rectus femoris, biceps femoris, and tibial anterior on each side. The first type of vibration feedback was a constant vibration of all six muscles. The second type was timed to the gait phase, each vibrator activated at the percentage of the gait cycle that the muscle is used. This experiment

showed that both types of vibration have a unique effect on the gait of the subjects. Constant vibration affects primarily the temporal parameters of gait, e.g., stride time. While timed vibration has a larger effect on the spatial parameters of the gait, such as stride length.

Chapter 1: DeepSole System Design

Gait analysis allows clinicians and researchers to quantitatively characterize the kinematics and kinetics of human movement. Sensor based gait characterization systems are recognized as clinical tools to analyze patient mobility[1]. For example, quantitative gait data has been used to determine the need for surgery in children with Cerebral Palsy (CP) and to prescribe the care and treatment after surgery [2]. Furthermore, Wren et at[3] showed that children with CP who underwent clinical gait analysis before lower extremity orthopedic surgery had significantly lower incidence of additional surgery.

Devices that quantify gait can be either portable, such as instrumented shoes, or non-portable, such as motion capture systems and instrumented walkways. There is a tradeoff between these two classes of systems in terms of portability and accuracy. The most accurate strategies to detect gait events using motion capture [4] or instrumented mats [5]. These devices are precise but are limited to lab settings. However, recent computer advances allow for the collection of meaningful data outside of the clinical setting, over different terrains and activities [6]. This is critical for recording abnormal walking behaviors, e.g., episodic phenomena like freezing of gait of patients with Parkinson's Disease [7]. Although the portable devices permit longer recordings in natural environments, the added flexibility increases the potential for sensor misinterpretation. This error can be significant when used on participants with irregular walking, such as the elderly, or individuals with CP, adding to the complexity of data processing.

Gait characterization typically includes both spatial and temporal parameters. These parameters can quantify changes in the user locomotion and can track progress of training or

rehabilitation. For example, stride to stride fluctuations can be used to assess risk of falls [8], [9] and gait variability has been used as a good predictor for dementia [10], [11].

To characterize the gait of a wide range of population, the DeepSole system shown in Figure 1.1 was created. This system consists of a soft, flexible insole which can be comfortably inserted into any standard footwear and an IMU mounted on the top of the footwear. It collects signals from twelve channels: three pressure signals, three linear accelerations, three angular velocities, and three Euler angles. The accelerations, velocities and Euler angles are measured in the local IMU coordinate system. The sensor readings are recorded on an on-board microSD card and streamed through Wi-Fi using UDP data packets.

Figure 1.1 Left, subject wearing the DeepSole system. Right, printed circuit board with microcontroller and IMU, and instrumented insole with pressure sensors (yellow outline) and vibration motors (green outline).

1.1 Insole Module

Each insole (Figure 1.2) consists of three pressure areas: one located under the phalanges, second located under the metatarsals, and the third located under the calcaneus. The pressure sensors are made with a layer of piezoresistive e-textile (Eontex, CA) in between two layers of conductive copper fabric. These sensors can be custom made to any shape and retain their

piezoresistive properties. The resistance of the fabric decreases when the applied load increases anywhere on the sensing area. By placing the sensors in the aforementioned locations, we can capture loading changes during the gait. The sensors provide an average loading of each independent area instead of just a single point. This feature is especially useful when characterizing populations with irregular loading during gait, such as children with CP.

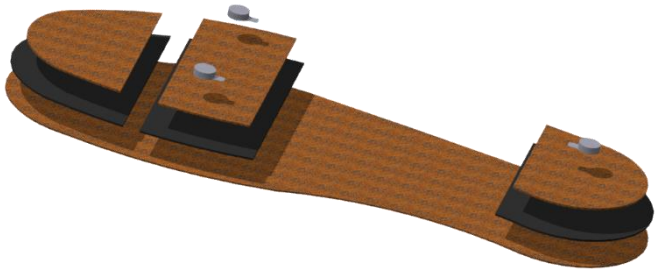

Figure 1.2 Exploded view of the right insole module. The bottom layer is conductive fabric connected to ground, the middle layer is piezoresistive e-textile, and the top layer is conductive fabric. The gray cylinders are coin vibrators.

The vibration motors are located under the first and fifth metatarsals, and the calcaneus. Each can be controlled independently to change the vibration intensity. The system can be donned in minutes and is similar to putting on a regular pair of shoes. Due to the soft materials used, the insoles are indistinguishable by the wearer.

1.2 Electronics Module

All the electronics are contained within a custom board of 40x45 mm, shown in Figure 1.3. The board connects to the insole module using an 8-pin connector. It consists of 6 submodules:

1) *Microcontroller*: A Photon (Particle, San Francisco) is an Internet of Things hardware development board. It has an ARM Cortex M3 microcontroller with integrated Wi-Fi, I2c communication, SPI communication, and 12-bit analog-to-digital convertor (ADC).

2) *IMU*: The 3-Space Embedded (Yost, Ohio) is 9 DoF inertial unit. It uses SPI communication and calculates the orientation at a frequency of 250 Hz with a $\pm 1^{o}$ accuracy.
3) *Micro-SD card writer*: The system can write all the sensors readings to a Micro-SD card. This allows the system to record long sessions without data loss.
4) *Pressure submodule*: consists of 3 voltage dividers connected to the ADC of the Photon. The resistances were calibrated to maximize the loading measurements.
5) *Vibrator submodule*: consists of 3 Mosfet transistors connected to Pulse-width modulation pins of the Photon. This allows the system to modify the intensity of the vibration as commanded.
6) *Charge management*: battery management integrated circuit that allows the system to run both on battery and USB power. This makes the system able to collect data for several continuous hours.

Figure 1.3 DeepSole board. Right is the front of the board; the Particle Photon is the main unit on this side. Left is the back of the board, the micro-SD card and the 3-Space Embedded IMU are visible

1.3 Data Recording and Transmission

The DeepSole system can record and stream data to up to 250Hz. All communication is done using the User Datagram Protocol, this protocol is used for time-sensitive communication where having the latest packet is more important than receiving all packets. Each packet is 37 bytes longs and contains a header, a footer, timestamp, 12 sensor readings, a sync flag, and the id of the shoe.

Each side can be controlled independently for data recording and vibratory feedback. To control the modules, a custom Graphical User Interface (GUI) was made using Python, shown in Figure 1.4. The GUI allows the user to control and monitor the system by showing the values of the sensors in real time.

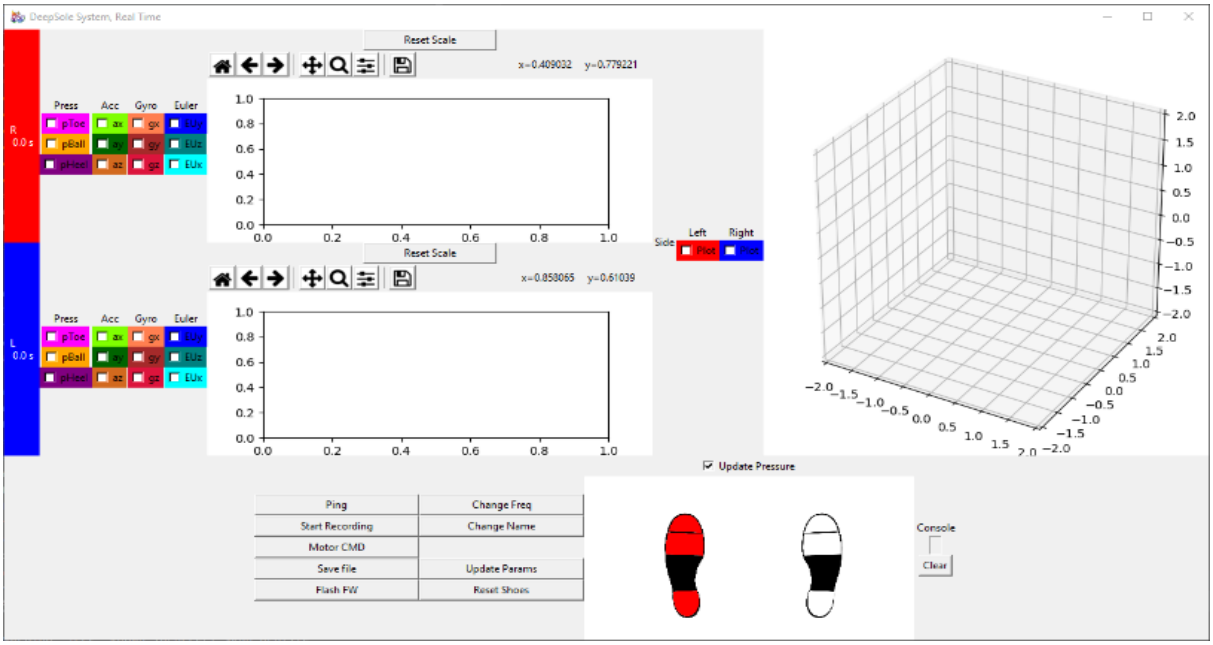

Figure 1.4 Graphical Interface to control the DeepSole system. The GUI allows to start/stop recording, change the data collection frequency, ping the boards. It also shows the values of the sensor signals in real time.

The two hardware modules along with the software for data transmission and recording. Allows us to use the DeepSole system with a wide variety of people. But the hardware and the software only provide raw sensor data. To use the data for gait analysis and training, it must be processed. This processing is commonly done manually by carefully designing algorithms that identify patterns and features in the signals. But this process is difficult, and it needs to be individualized for each subject.

In the incoming chapters, artificial neural networks will be explored as a replacement for the manual processing of the sensor data. Artificial neural networks can be applied as universal approximators for mapping one domain to another. They are computationally expensive during training, but once trained, they are an efficient method for domain mapping.

Chapter 2: Neural Networks for Gait Segmentation

Wearable devices can make gait analysis convenient and portable [12], allowing data collection for characterization and long-term monitoring in any environment [13]. State-of-the-art wearable devices use e-Textiles and flexible electronics [14] to conform to the shape of the user, minimizing impact on their motion. Wearable devices tend to be less accurate than their laboratory counterparts [15], making it challenging to use for gait measurement without any preprocessing.

To analyze the gait data collected, most techniques involve two stages: (i) segmenting the data into steps or strides to calculate temporal parameters, then (ii) estimating the spatial parameters using the segmented data.

The initial contact time, usually made by the heel, is set as the start of the gait cycle [16]. Different algorithms have been proposed to obtain gait. These methods analyze the sensor readings but require human effort to validate and "clean" the data, e.g., for removing sensor errors or noise. This is a time intensive step and prone to errors as only a limited number of features during the sensor measurements can be considered, e.g., pressure or inertial measurements. The methods mentioned above provide good performance but rely on the skills of a person analyzing the data to find the important features in the recorded gait. Also, algorithms need to be formulated to identify these engineered features. The difficulty of finding these features increases as the number of sensors grows. However, limiting the number and types of sensors introduces the risk that data cannot be processed if the device malfunctions.

Various algorithms for wearable devices using thresholding [17], rule-based [18], or machine learning [19] have been proposed to identify gait events. Han et al. [20] used an IMU at the shank to identify normal/abnormal HS and TO using a rule set based on the angular velocity

and acceleration with a reported accuracy of 94%. Karuei et al. presented a rule-based method to analyze walking cadence with a smartphone at a rate of 0.5 Hz [21]. Delgado-Gonzalo et al. used an accelerometer and ruled-based algorithm to estimate gait parameters at a frequency of 1.0 Hz [22]. Given than the average human gait is 2 Hz [16] and these methods vary in accuracy and latency, some are unsuitable for continuous gait training.

Machine learning allows to automate tedious processes and greatly reduces the time needed to obtain meaningful output data. Hannink et al [23] used Convolution Neural Networks to obtain spatiotemporal gait parameters from an inertial sensor with performance comparable to state-of-the-art devices. Manini et al [24] created a gait segmentation algorithm using Hidden Markov Models (HMM) with signals acquired from a gyroscope mounted at the foot. They obtained an accuracy of 98.3% when considering an event identified by a rejection window less than ±30 ms. For their experiment, they used only three healthy participants walking on a treadmill for two minutes at various speeds and inclines.

Lopez-Nava et al[25] used a Bayesian model to estimate the temporal gait parameters of ten healthy participants over three 7.6 m laps at a comfortable walking speed. Only the acceleration data was recorded and processed, showing an accuracy and precision (absolute error ± standard deviation) of 9.1±6.5 ms for step time, 42.3±20.2 ms for stance phase time, and 32.2±13.9 ms for swing time.

Artificial Neural Networks (ANN) allow the mapping of an input vector X to an output vector Y, where the input and output can be multidimensional [26]. The algorithm looks at a single event through different sensors and merges this information in their mapping, thus avoiding the need to manually program algorithms that recognize engineered features. For time-series data, the ANN commonly used are either Convolutional Neural Networks (CNN) or Recurrent Neural

Networks (RNN). CNN are specialized for processing data that have a grid-like topology [27], and have been successfully used to identify human motion from the signal of several Inertial Measurement Units (IMU) [28]. RNN are models with the ability to sequentially process information one element at a time, generating a sequence-to-sequence mapping [29]. They excel at determining outputs from inputs that are not independent [30]. RNN are more desirable than CNN because they accumulate data, capturing long-range time dependencies [30].

Segmentation is the step of gait analysis that involves splitting the data into cycles. Each cycle is defined by Heel Strikes and Toe Offs. Even though several algorithms exist to identify these events, they usually involve supervision and intervention from a human to identify faulty cycles. False positives can come either from sensor errors, or from gait variability of the participants. Identifying faulty cycles is time intensive and could take the user between 1 hour to 12+ hours to analyze 6 minutes of walking data of each subject.

Using HS and TO, we can segment data and calculate 15+ spatial gait parameters. A graphical example of the different gait events and how to identify these using only HS and TO events is shown in Figure 2.1. With our proposed algorithm, we wish to substitute commonly used thresholding algorithms to segment the data. The thresholding algorithms are ineffective when the user has an abnormal gait, as the pressure data can be erratic, and a single threshold value may not be sufficient for the entire recording.

A model specifically created to reliably identify and characterize a person's gait using the raw data, without any pre-processing, the time needed to obtain meaningful data would be greatly reduced. This would allow researchers and clinicians to record and analyze long walking sessions outside the clinical environment. However, it is critical for the model to maintain equivalent

accuracy and precision when compared to the state-of-the-art methods, while still significantly reducing the processing time.

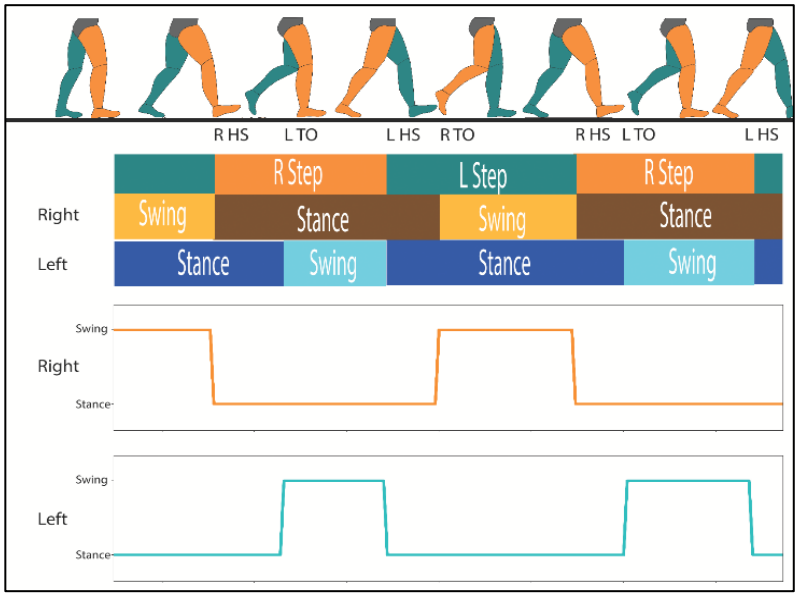

Figure 2.1 Top: a graphical representation of a normal gait cycle and how the events are defined by heel strikes and toe off. Bottom: an example of a binary function of the gait phases.

To achieve this, an RNN model that classifies the recordings from an instrumented shoe was designed. The model output is used to segment the walking data and to calculate temporal characteristics of the gait. RNN was chosen over CNN because it provides an output for every intermediate step of the network[26]. This model property was used to reduce the number of incorrect predictions. The input to the network is the data of three pressure sensors, a 3-axis accelerometer, and Euler angles of the feet. Here, we show that using the RNN classifier, we can segment the walking data within seconds without human intervention.

2.1 Dataset Description

The dataset used for the training and evaluation of the model consists of 28 healthy participants over 18 years old (8 females and 20 males, age 19 to 31). A second dataset of 7 children

(4 females and 3 males, age 7 to 14) with CP was collected and used for evaluation. Participant characteristics are listed in Table 1. Since the experiment of walking with shoes is non-invasive, the only requirement to participate in the experiment was the ability to walk independently for 6 minutes. None of the participants used assistive devices during their testing.

For the CP group, the inclusion criteria were that they were diagnosed with unilateral CP, were able to walk for 6 min without any assistance, cooperative, and aged between 6 and 17 years old. People that presented other neurological disorders, e.g., orthopedic surgery or botulinum toxin injections on the affected leg within 6 months were excluded from the experiment.

Table 1 Participant Characteristics for CP Group

ID	Height(cm)	Weight (kg)	Shoe	Gender	Age	Affected Side	MACS	GMFCS	Lesion Type
CP001	185	94	12	M	15	Left	II	I	MCA
CP002	170	52	12	M	14	Left	II	I	PVL
CP003	132	24	6	W	10	Left	II	II	PVL
CP004	152	52	6	W	12	Right	I	I	MCA
CP005	137	42	5	W	8	Left	III	II	PVL
CP006	138	27	5	W	9	Left	III	II	PVL
CP007	155	33	7	M	14	Left	II	I	PVL

The participants were asked to perform the 6-minute walk test (6MWT) [31] while wearing the DeepSole system. During this test, a subject walked at a self-selected speed for 6 minutes in a hallway equipped with a Zeno Walkway (Protokinetics, PA). The walkway has a total length of 6m, but 2m were added to the extremes of the walkway to make a total walking distance of 10m. Data was recorded simultaneously from both systems. Parents and children signed informed consent/child-assent forms approved by the Columbia University Medical Center Ethics Committee.

2.2 Architecture Design

From the DeepSole, we obtain nine signals: three pressure sensor readings, three linear accelerations, and three Euler angles. The last 20 readings from the sensors are appended into a matrix $X \epsilon \mathbb{R}^{20x9}$ to use as inputs to the RNN. Here, the columns represent the values of the signals and the rows represent the time when the signals were recorded. The last row is the current reading at time (t) and first row is the readings at time $(t - 19 * d_t)$, where d_t is the sampling time of 10 ms. In the training set, the left and right-side recordings were used indiscriminately. This allowed the model to classify the data using information only from the desired side. This should make the model suitable for predicting symmetric and asymmetric gait, as each side is predicted independently.

Since HS and TO are very short time events, creating a model to identify these events would be impractical. Therefore, the gait cycle was split into the phases of a step and the HS and TO information were later reconstructed from this output. Using this approach, we can obtain several training samples from a single step instead of only 2 per step, one for HS and one for TO. The Network is an RNN classifier with two classes: stance phase and swing phase. Using this strategy, the model can generate a function of time showing the phase of the gait. By using the differentiation of the output, we can identify HS as going from off the ground to on the ground ($\dot{y} = -1$), and TO as the point where the foot is no longer in contact with the ground ($\dot{y} = 1$).

The output of the network is a binary function of time that shows the phases of the gait:

$$y(t) = \begin{cases} 0 & Stance\ Phace \\ 1 & Swing\ Phase \end{cases} \quad (1)$$

Figure 2.2 shows a schematic of the model's architecture. First, the input matrix is normalized per channel and is fed into a RNN containing 8 layers, each with 20 Gated Recurrent Unit (GRU) cells[32].

From the RNN, we obtain a matrix $R \epsilon \mathbb{R}^{20x20}$, where every row i corresponds to the predicted value of $y(i+1)$, and $i = 20$ is equivalent to the current time[29]. This matrix is used in the classification layers.

The model splits into two outputs, one part gives the expected values for $y(t)$ to $(t-10)$ using rows $i = 9$ to $i = 19$ from matrix R and the following equations:

$$j = 19 - n \tag{2}$$

$$y(t-n) = \text{argmax}\left(\text{softmax}\left(R_j W_j + b_j\right)\right) \tag{3}$$

where $y(t-n)$ is the predicted value at time $t-n$, R_j is the j^{th} row of matrix R, $W_j \epsilon \mathbb{R}^{20x2}$ is a weight matrix and $b_j \epsilon \mathbb{R}^{1x2}$ is a bias vector.

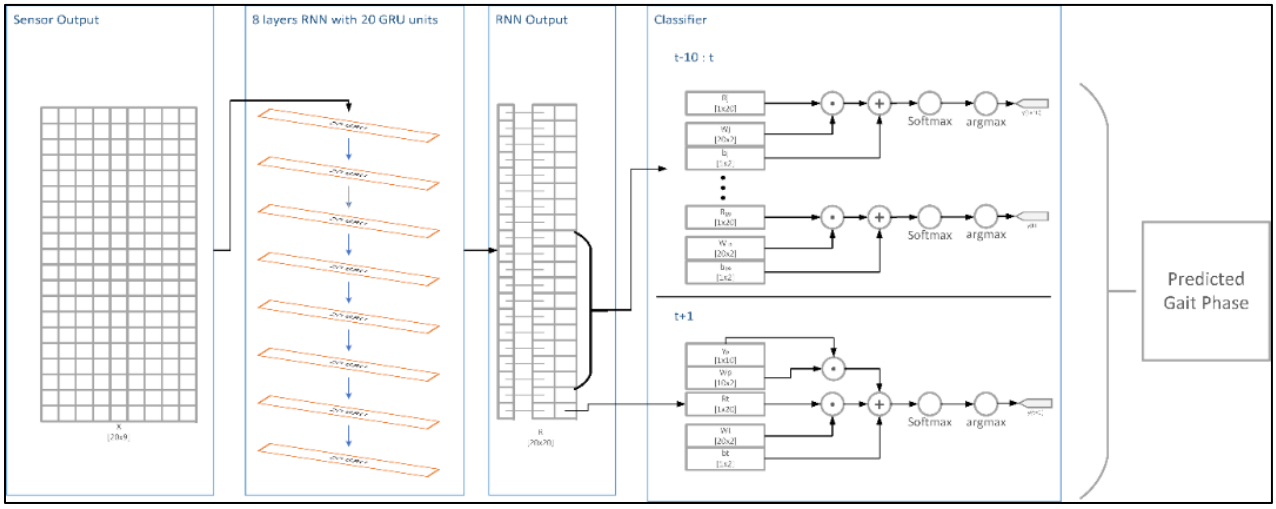

Figure 2.2 Network Architecture for the segmentation model. Sensor measurements are fed to an RNN with GRU units, the output is then passed through a classifier to obtain the prediction for t+1

The second output predicts the value of $y(t+1)$ by considering the previous values of y using:

$$y(t+1) = \text{argmax}\left(\text{softmax}\left(R_t W_t + y_p W_p + b_t\right)\right) \quad (4)$$

$$y_p = \begin{cases} y_{true} & if\ training \\ y_{predicted} & if\ evaluation \end{cases} \quad (5)$$

where $y(t+1)$ is the predicted time for the next location of the foot given the past 20 sensor readings, R_t is the last row of matrix R, $W_t \epsilon \mathbb{R}^{20x2}$, $W_p \epsilon \mathbb{R}^{10x2}$ are weight matrices and $b_t \epsilon \mathbb{R}^{1x2}$ is a bias vector. y_p is a row vector containing the last 10 values of the output $y(t)$. During training, these values are fed from the training set, but during run and evaluation the predictions obtained from Eq. (3) are used.

In equations (3),(4) the SoftMax activation and the argmax combined create a "1-of-2" encoding, winner-takes-all of the outputs[33]. The SoftMax function is used to represent the probability distribution over two classes[27] and argmax is used to choose the class with the highest probability.

Each model was trained over 200 epochs, i.e. the model goes 200 times through the dataset using an Adams optimizer[34] to minimize the cross-entropy loss function (6).

$$H_{y'}(y) = -\sum_i y'_i \log(y_i) \quad (6)$$

2.3 Model Evaluation

The model presented is a classifier of the gait phase, i.e., 0 for stance and 1 for swing. To obtain meaningful gait characteristics, one must identify the HS and the TO events.

Given the model architecture, at every time t, two outputs are provided, the predicted phase and the expected phase for the last 10 measurements. This means that after 10 system cycles, at every time t, there are 10 values for the position of the foot at time t. By rounding the mean of all ten predictions, the output can reduce the number of false predictions. This is particularly useful at the HS and TO gait events since these are located at the transition between states and should be singleton events per step cycle.

To test the performance of the algorithm, a "leave-one-out cross-validation" (LCV) test was performed over the P participants (P=28). A total of P models were trained with P-1 participants[35]. The LCV was repeated P times excluding a different subject for every iteration. For each of the P models created, the dimensions of the training datasets were kept constant by randomly selecting 5000 samples from each subject (2500 stance phase and 2500 swing phase samples). Using 5000 samples per subject means that for training, we are only using 50 seconds out of the 6 minutes recorded. By decoupling the effects of the participants involved in the training, this cross-validation allows performance evaluation of the learning ability of the network architecture.

Two participants were selected and tested with each model (28 participants for each group). The participants were divided into two categories: In-Training (IT) and Not-In-Training (NIT). NIT members are the participants left out of the training for the model tested. IT were participants, picked at random, whose step information were used during the training of a model. Each subject was tested two times, once as part of IT and once as part of NIT. If the classification performance of the network and error ranges are similar between groups, the model could be used with unknown participants, within the same population, without the need for a calibration session.

The model with the highest test accuracy was used with a dataset of 7 children with CP. To assess the performance of the RNN, the HS and TO identified were compared against the walkway recording. Each event was paired using a maximum search window of 0.5 seconds to identify the corresponding step. Each event required the HS and TO to be identified. If any was missing, the event was counted as unidentified and was not used for the error calculation. The mean errors (ME) and mean absolute errors (MAE) were used to quantify the accuracy and precision of the RNN.

2.4 Results

During the training, the 28 models achieved a mean accuracy (ME ± SD) for classifying the gait phase (Eq. 1) of 91.45±0.27% for y at time $t+1$ (Eq. 4), and 91.03±0.21% for y_p (Eq. 3) at time $t-9$ to time t on the training dataset. For the test dataset, the mean accuracy was 89.20±4.73% for $y(t+1)$ and 89.08±4.64% for y_p.

The model was able to identify 4138 out of 4198 steps for NIT comparison, each step a HS and TO, for 28 participants over 6 minutes of walking; this is a 98.6% identification rate. For the IT group, it identified 99.4% of the steps (4174). For the CP group, the RNN identified 1776 out of 2192 steps for the 7 participants; this is an 81.0% rate.

For the NIT group, the model was able to achieve an accuracy and precision (ME ± SD) of -5.9 ± 37.1 ms for HS and 11.4 ± 47.4ms for TO. The IT group achieved an accuracy and precision of -8.3 ± 23.5 ms for HS and 10.7 ± 42.3 ms for TO. For the CP group, the model achieved 26.4± 46.0 ms for HS and 21.0 ± 94.6 ms for TO. Results showing the mean error and the RMSE are presented in Table 1 for both healthy groups tested and for the CP group.

The error histogram and the Bland-Altman plots[36] between the RNN and the reference system for the three groups and the two events are presented in Figure 2.3 and Figure 2.4. The Bland-Altman plots show that the performance of the NN is maintained over the complete recording.

Table 2 Results by Group and Event in Milliseconds

Event	NIT		IT		CP	
	ME ± SD	MAE ± SD	ME ± SD	MAE ± SD	ME ± SD	MAE ± SD
HS	-5.9 ± 37.1	23.9 ± 29.0	-8.3 ± 23.5	16.8 ± 18.5	26.4± 46.0	35.2 ± 39.7
TO	11.4 ± 47.4	35.9 ± 32.8	10.7 ± 42.3	32.8 ± 28.7	21.0 ± 94.6	68.6 ± 68.6

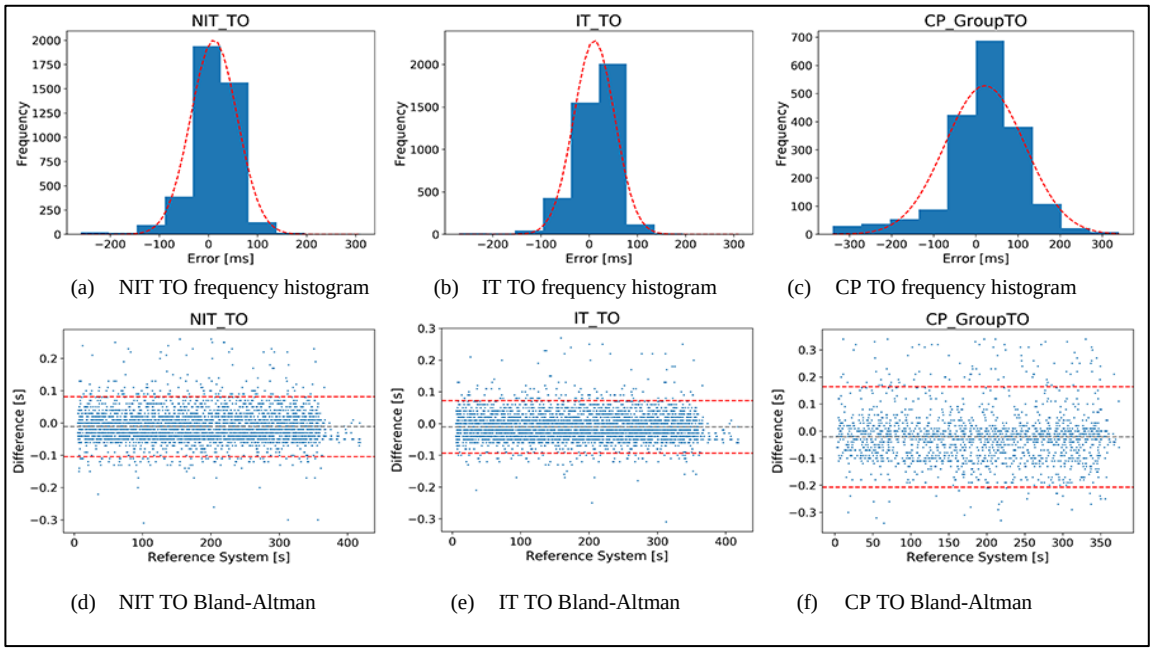

(a) NIT TO frequency histogram (b) IT TO frequency histogram (c) CP TO frequency histogram

(d) NIT TO Bland-Altman (e) IT TO Bland-Altman (f) CP TO Bland-Altman

Figure 2.3 Error distributions of the identification errors for TO with respect to the reference system. 5a, 5b, and 5c show a histogram of the error distributions for the three groups. The Bland-Altman plots showing the bounding error for TO for the NIT, IT, and C

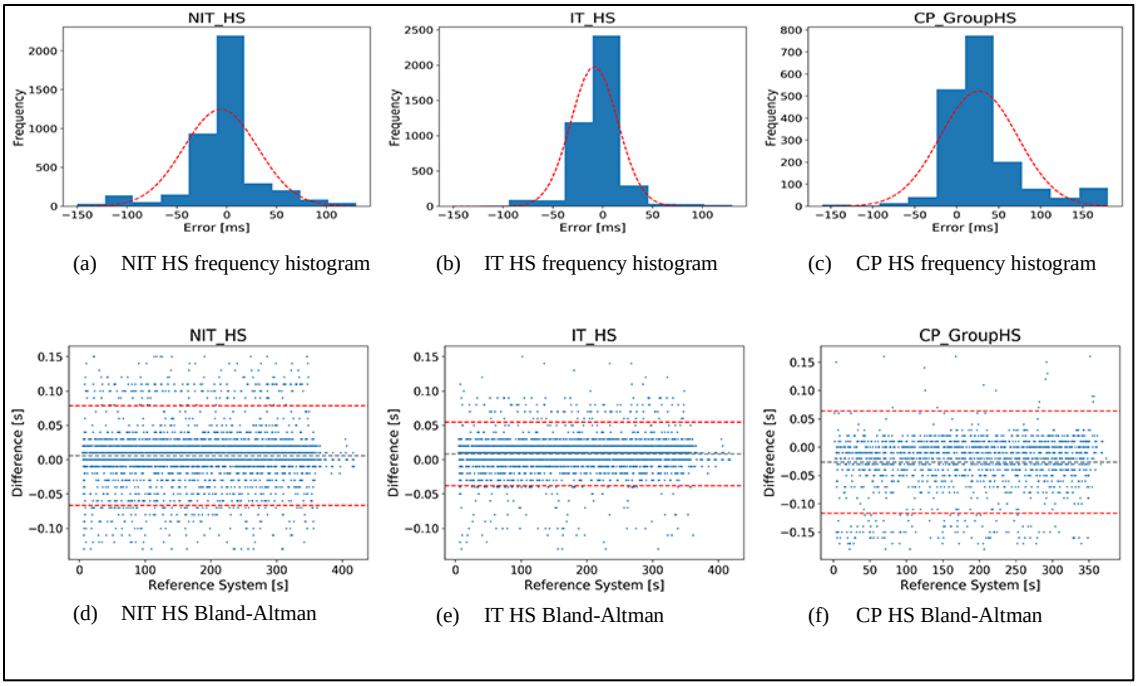

(a) NIT HS frequency histogram (b) IT HS frequency histogram (c) CP HS frequency histogram

(d) NIT HS Bland-Altman (e) IT HS Bland-Altman (f) CP HS Bland-Altman

Figure 2.4 Error distributions of the identification errors for HS with respect to the reference system. 4a, 4b, and 4c show a histogram of the error distributions for the three groups. The Band-Altman plots showing the bounding error for HS for the NIT, IT, and CP

2.5 Discussion

The algorithm was tested with dataset of 28 adult participants and 7 children with CP. The model was able to utilize the full range of sensors to segment the data even when sensor error was present, Figure 2.5. The classification capabilities were maintained when the subject was not involved in the training. This was tested using LCV; the precision and accuracy were maintained between the NIT and IT groups. This means that the RNN architecture learned to classify the gait by using the multi-dimensional space created by the pressure and inertial sensors and could be used without subject specific calibration for the healthy group and further testing is need for other populations.

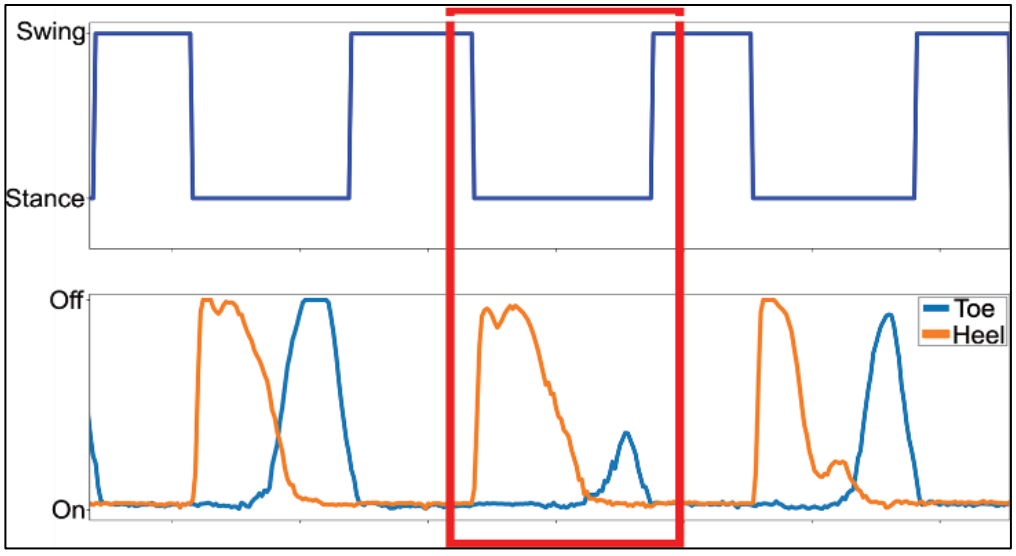

Figure 2.5 Sensor error due to variability in the walking characteristics of subjects. RNN Model can classify the data despite the misreading. Only Heel (calcaneus) and Toe (distal phalanx) are shown for clarity

The results in this study show that the algorithm presented, based on RNN for segmentation and estimation of temporal parameters of gait, provides reliable performance compared to a commonly used instrumented walkway when tested with healthy adults. Furthermore, it has a similar accuracy and performance to other Machine Learning algorithms that use techniques like Hidden Markov Models or Bayesian Models, even when it was tested with over 200 minutes of walking.

Even though the RNN had a diminished accuracy and identification rate when used with children with CP, the results are encouraging. Especially, when we consider that the RNN was trained with young adults and it had never seen data from children, let alone those with CP. As shown by Wren et al[37], children with CP often present with gait abnormalities such as equinus and calcaneus, and in-toeing and out-toeing. This makes processing the recordings even with a reference system challenging and time consuming, since it involves manual correction. With the RNN, the processing of all 7 participants took only seconds. This means that the algorithm may

be used with long recordings outside of a clinic environment, where even an 80% detection rate can still provide the overall trends of the gait. Also, we believe that by increasing the number of participants with CP and combining the datasets between adult and children participants, we can create models usable on both populations.

The presented model can be use not only to segment gait data into strides and steps. It can also be used to provide feedback at specific events or during specific gait phases. Although, given that the output of the model is a discrete signal it would not be useful for close-loop feedback that require continuous tracking of the gait.

Chapter 3: Neural Network for Gait Cycle Percentage Prediction

While the algorithm presented in the previous chapter can be used to identify specific gait events, like Heel Strike (HS) and Toe Off (TO), that are widely used in event-detection-based open-loop feedback strategies.

A better metric for continuous gait training would be gait cycle percentage. The gait cycle begins at a heel strike (HS) of one foot and ends at the next HS of the same foot (Figure 3.1). It is comprised of both stance and swing phases [38]. Stance phase typically occurs from 0 to 60% of the full stride. It is the period when a foot is in contact with the ground, from the HS to toe off (TO) of the same foot.

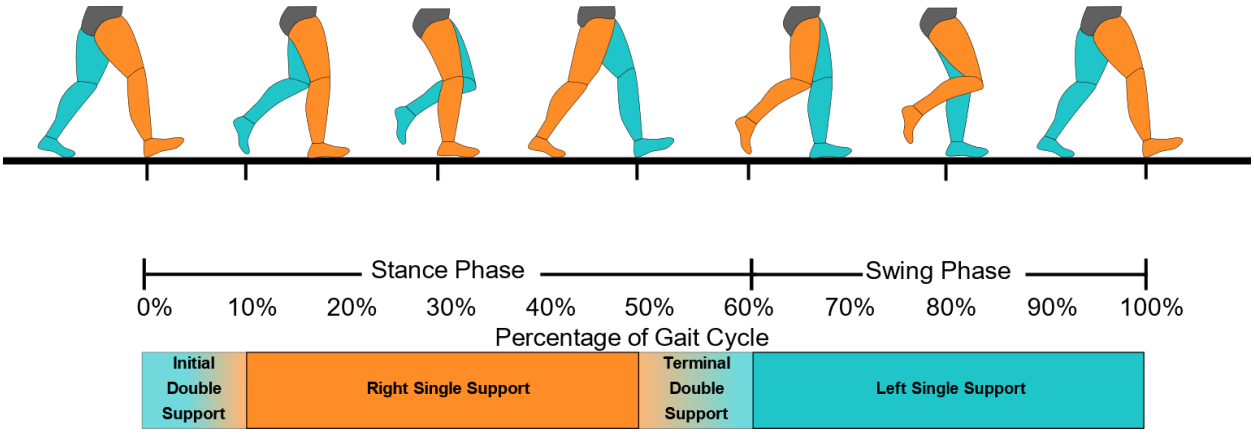

Figure 3.1 The phases and events in a normal gait cycle, including gait events like Heel Strike and Toe Off, and Single and Double support stages.

For continuous prediction of a cyclic motion, one method commonly used in gait-assistance devices is an Adaptive Frequency Oscillator (AFO). This method uses oscillators to predict the cycle percentage of pseudo-periodic signals. Some algorithms use pressure sensors to detect the start of the cycle [39], and some can detect the start with a single periodic signal [40]. These

algorithms can adapt to changes of cycle frequency but require a few cycles to achieve it. AFO is frequently used to control exoskeletons [41]–[43], where the signals of sensors are used to identify the current gait percentage and modify the feedback or controller accordingly.

One way to accurately track gait cycle, despite sudden changes in the gait, is by using an Artificial Neural Network (ANN). Using a training dataset, ANNs can automatically identify patterns in the signals and map these to a desired output function. ANNs use stochastic gradient descent and backpropagation [44] to optimize the weights in the network. This property allows the network to analyze several arrays of sensors in a single step.

Identifying gait characteristics from raw sensor signals is challenging, as these vary for each individual due to physiological differences and walking environment [45]. However, the general patterns in the sensor signals remain the same over the cycles for typically walking individuals.

Convolutional Neural Networks (CNN) use convolution to find the kernel parameters automatically, reducing the noise by encoding and decoding the data [27]. It has been used to identify human motion from IMU signals [28].

Recurrent Neural Networks (RNN) capture time dependencies in the data and generate sequence-to-sequence mapping [29]. RNN models use leaky units to help the network maintain its state, accumulate data over time, and forget the previous states when they are no longer relevant [27].

ANNs have also been used for continuous gait tracking. Vu et al [46] used an Exponentially Delayed Fully connected Neural Network (ED-FNN) to predict the gait cycle percentage with a resolution of 1%. Using a dataset of seven healthy subjects, they achieved a performance of 0.01 mean square error (or 10% Root Mean Square Error) on a dataset of 7 healthy young adults. They

used this network to predict the gait cycle with a resolution of 1%. Although their results are promising, the validation of their network was done with the data of the same subjects who were used in the training. In this strategy, baseline data is needed for each new subject to achieve the reported performance online. This extra baseline session can prove difficult for subjects with gait abnormalities which limit the amount of continuous walking they can do. Furthermore, if the target of the training is to modify the gait with respect to the baseline, the calibration might not be valid for all training sessions.

Since ANNs treat each sample as an independent event, they do not require any prepossessing between subjects or side. Also, the network can respond immediately to changes in cadence. These properties make ANNs an attractive method to track the gait during training, where the goal is to change the typical gait of the patient. Furthermore, if the training dataset has sufficient inter-subject variability, this model could be used to predict novel subjects. This is a great advantage over methods like AFO and rule-based algorithms.

To improve the gait cycle percentage prediction, an algorithm which predicts the percentage of the gait cycle using an ANN was created. This novel algorithm uses an Encoder-Decoder RNN architecture that combines the filtering features of a CNN with the time series processing features of an RNN to predict the gait cycle percentage in real-time. We show that this model handles the raw data from 3 different sensed features (3 pressures, 3 accelerations, and 3 rotation angles) and accurately predicts the gait. To validate the performance of the model and the effects of the different layers, an analysis was performed with data recorded from 24 healthy adults wearing the DeepSole system [12] shown in Figure 1.1. Using leave-one-out cross-validation (LCV) [35], we tested the performance on subjects that were not included in the training. LCV can

show the performance of a pretrained model on a new subject without any calibration or baseline recording.

3.1 Dataset Description

The training dataset contains gait data from 24 healthy participants, 6 females and 18 males (age 25.1 ± 4.6 yrs., height 1.7 ± 0.09 m, weight 75 ± 4.6 kg). The participants walked for 6 mins on a 7 m long instrumented Zeno Walkway (Protokinetics, PA, USA). Each participant walked multiple continuous laps on the instrument walkway. Once the participant reached the end of the mat, they would turn around and walk back. This was repeated for the duration of the recording. Data were collected concurrently by the DeepSole system and the Zeno Walkway and were synchronized by sending a User Datagram Protocol (UDP) packet to the footwear when the Walkway started recording.

Signals from the DeepSole were originally collected at 200 Hz. However, to decrease the computational load, the training set was down sampled to 100 Hz. Signals from each subject were segmented to samples of 50 continuous time points as inputs to the neural networks, i.e., 50 data points at 100 Hz corresponds to a moving window of 0.5~s. We treat each sample as independent from one and other. The gait data from the Zeno Walkway were collected at 120~Hz and were used as the ground truth. The gait cycle percentage was calculated from HS to next HS of each side, as detected by the walkway. From each subject, 5,000 samples were randomly selected as training data (2500 samples were from the left foot and 2500 from the right foot).

3.2 Architecture Design

Three ANN modules were evaluated to find the properties that they provide to the prediction. All modules received and output a 3D tensor, where the first dimension corresponds to the batch, the second to the time, and the third to the features.

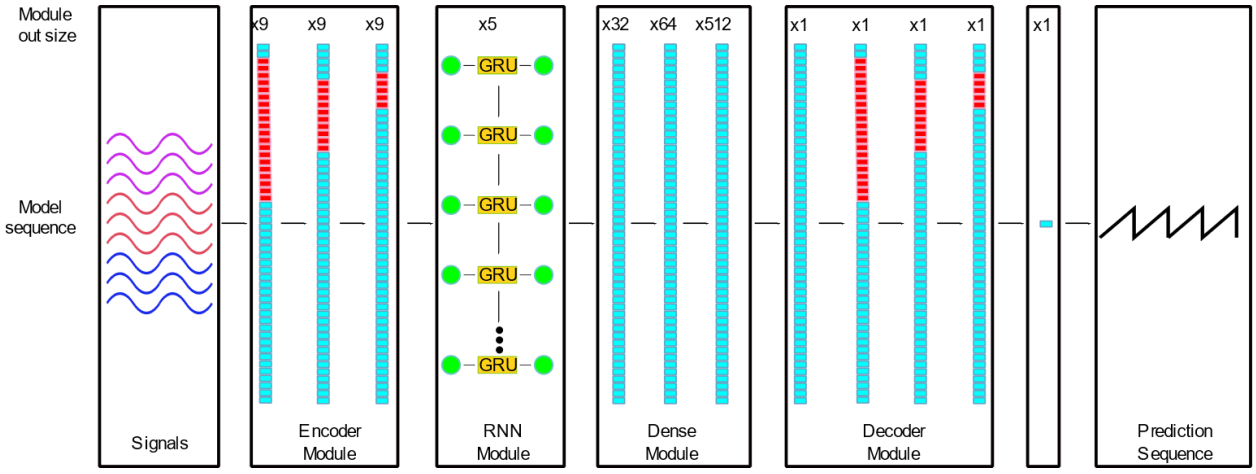

Figure 3.2 Graphical overview of the neural network modules in the Encoder-Decoder RNN model. ERM is an encoder-decoder RNN that maps the 9 signals collected by the DeepSole system into the predicted gait cycle percentage. A 0 value corresponds to gait cycle start

The dense module consisted of 3 fully-connected layers with 32, 64, and 512 neurons, respectively. Each layer used a rectified linear unit (ReLU) [47] activation. The weights were shared across the time dimension of the data.

The RNN module consisted of one recurrent layer with 5 Gated Recurrent Unit (GRU) cells [48]. Since this layer is capable of processing data sequentially and we wanted to predict the gait percentage for the next sample time, the data was processed forward. The recurrence was performed along the second dimension of the tensor.

For the Encoder-Decoder (ED) module, three 1D convolutional layers with kernel sizes of 20, 10, and 5 were used to encode signals from each channel independently. The length of the

tensors was fixed throughout the convolution by using the number of features of the input tensor as the number of filters. The convolution output was fed into the next module and then fed to a dense layer with a filter value of one, and then three 1D convolutional layers with kernel sizes of 20, 10, and 5 to decode the output. For all convolutions, a padding was done to keep the dimensionality of the input and a ReLU activation was applied after each layer.

The last layer for all model sequences was a fully-connected layer with a single neuron. The input to this layer was flattened and sigmoid activation was used to ensure that the output was bounded between 0 and 1.

The Encoder-Decoder RNN model (ERM) presented uses the Encoder module, then the RNN module, followed by the dense module, Decoder module, and finally the last module. This architecture is shown in Figure 3.2. The hypothesis is that this model which combines all 3 modules in a single model will have the best prediction performance. This is similar to the Encoder-Recurrent-Decoder model proposed by Fragkiadaki et al. to predict human body pose from video data [49].

Dropout was used throughout the model to avoid over-fitting [50]. To train the network, mean absolute error was optimized by applying the Adam optimizer [34].

3.3 Methods

To test the algorithm accuracy and precision on novel subjects, a LCV test was performed [35] over P (P = 24) subjects. P models were trained using 5,000 samples from P-1 subjects for 500 epochs. The validation dataset was the full recording from the subject that was left out and it was used to evaluate the performance of the model.

3.3.1 Algorithm Evaluation Parameters

The model should predict gait percentage accurately. This prediction should be sufficient to correctly identify and segment strides in a timely manner. To measure the algorithm's performance, four critical parameters were identified.

Root Mean Square Error (RMSE) was used to measure the accuracy and precision of the predicted gait cycle percentage.

To identify the HS, or beginning of the cycles, the first and second derivatives of the prediction were used. At the end of the cycle, the first derivative is negative, and the second derivative is positive. This is because the percentage changes drastically from 100% to 0%, then increments steadily. Using this property, we can identify the false positives as the moments where these conditions are met, but there is no HS. False negatives were considered when a HS occurred, but the derivative conditions were not met. The quantity of false positives and negatives are measurements of the segmentation capability of the algorithm.

Lastly, to calculate HS detection delay, the predicted HS were paired with the ground truth HS. The time difference between these events quantifies the prediction delay.

3.4 Results

A total of 18,840 strides were used to measure the performance of the model. The strides were from both the left and right sides of all 24 subjects. Each of the evaluation parameters were calculated by comparing the entirety of each model's predicted gait cycle percentages with the ground truth. Therefore, for each model there are 24 values per evaluation parameter. The average of these performances is taken. For example, the reported lag for ERM is the average lag of the ERM model compared to the ground truth of all subjects.

The model had an RMSE accuracy (mean ± sd) of 7.2 ± 2.4 % with a distribution (median ± IQR) of 6.1 ± 3.6 %. The frequency accuracy of False Positives was 8.3 ± 7.3 % with a distribution of 7.3 ± 9.0 %. The frequency accuracy of False Negatives was 0.5 ± 1.3 % with a distribution of 0.1 ± 0.5 %. For Event ID Lag, the accuracy was 41.5 ± 24.7 ms with a distribution of 23.5 ± 44.9 ms. Figure 3.3 shows the box plots of the performance of the model for all metrics evaluated.

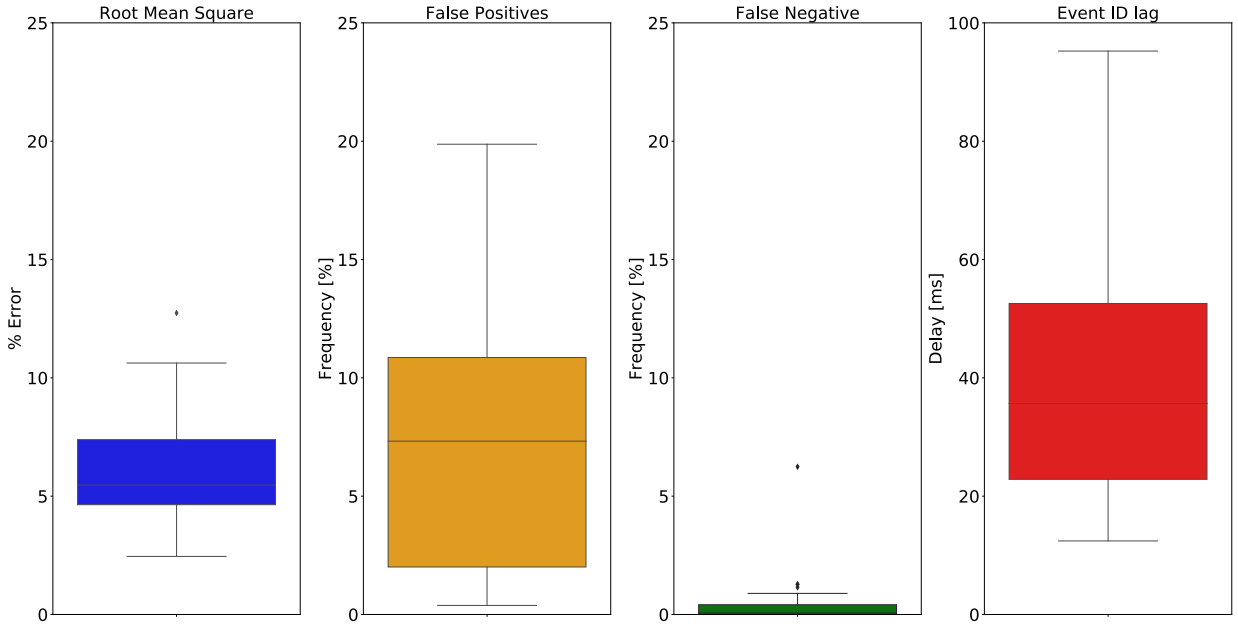

Figure 3.3 Box plot of the evaluated parameters for the ERM model. From right to left, Root Mean Square Error, False Positives, False Negatives, Event ID lag

3.5 Discussion

Adding the Encoder-Decoder module to the RNN and Dense modules (ERM) significantly reduces the RMSE of the predicted percentage of gait compared state-of-the-art. The ERM has small RMSE and the low variability between subjects. Combining the Encoder-Decoder with the

other modules also reduces the HS identification lag, as the ERM lag is significantly lower than that of RM. Moreover, it has a low number of false positives and false negatives.

Table 3 shows a comparison of the ERM with the state-of-the-art. The ERM has better performance in the HS identification lag than ruled-based [18] and HMM [19] methods. ERM has comparable performance to the ED-FNN [46], but the dataset used for testing is larger and the performance was tested with novel subjects.

Table 3 Comparison with State-of-the-art for Event ID lag and RSME. Bolded rows are the presented model

Method	Type	Performance	Metric	Baseline Required	Dataset size
H. F. Maqboolet et al [18]	Ruled-based	17 ± 11 (HS)	Mean ± sd	Yes	4
A. Mannini et el[19]	Hidden Markov Model	-16 ± 15 (HS)	Mean ± sd	No	9
A. Prado et al	Presented Model	4 ± 31 (HS)	Mean ± sd	No	24
H. Vu et al [46]	Neural Networks	10 %	RMSE	Yes	7
A. Prado et al	Presented Model	7.2 %	RMSE	No	24

By using the LCV method, we can assess the performance of the model on novel subjects without any calibration. This is an improvement over state-of-the-art methods that require a

baseline recording for parameter tune up. Removing the need for a baseline recording could be critical when the subject has gait abnormalities and is only able to walk for a short period of time.

Using supervised learning, this method is scalable, allowing an increase in the number of sensors in the system without increasing the complexity. Having redundancy of sensors is desirable in wearable devices, as the onboard sensors are more sensitive to environmental noise. The ERM architecture can be easily maintained, only needing tune ups of neurons and CNN filters. With other types of algorithms, the engineered features must be identified for each sensor, type of gait, and environment, which increases the complexity and computational load of the algorithms.

Using ERM to predict gait, we treat each sample as an independent event. This means the model would retain the predictive capability when two concurrent strides differ. Other methods, like AFO, depend on a rolling average of the last *n* strides for accuracy. With ANN, each sample is independent. Therefore, it does not need to adapt to changes in frequency. Furthermore, this paradigm can also be applied to other human motions which are not cyclic.

3.6 Conclusion

This work shows that the combination of all modules into a convolutional encoder and decoder can be used to accurately learn the temporal correlation across a time sequence. The RNN was used to learn the temporal dynamics from multi-channel time series signals. This model can be used to predict the gait cycle percentage within 7% RMSE. Even though the subjects in the study had different cadences, the models were able to continuously predict the gait of the subject for both left and right sides.

The presented method was only tested with healthy individuals, but it is capable of accurately predicting the gait phase of all subjects in the dataset, regardless of their gender, height,

or weight. Although, the model was only tested with straight walking and a limited number of subjects, the proposed method could be expanded to other population and gaits by using a broader dataset.

The left and right side are treated as independent. This means that a subject could have long strides on the right side and short strides on left and this would not affect the model's performance. This opens the door to training with a variety of patient populations with asymmetric gaits, such as individuals with Cerebral Palsy and stroke survivors.

In the last two chapters, algorithms were presented that map the raw sensors of the DeepSole system to gait parameters. These parameters were tested with both normally developed adults and children with Cerebral Palsy. But other gait related events or phenomena can also be mapped. In the next chapter, this will be explored by using the raw sensor data from the system to identify and episodic event know as Freezing of Gait.

Chapter 4: Neural Networks and Freezing of Gait

Parkinson's disease (PD) is the second most common neurodegenerative disorder in the world, affecting about 1% of the population over 60 years of age [51]. Depending on the stage of the disease, between 20-60% of individuals with PD suffer from episodic freezing of gait (FoG) [52]. FOG is a motor phenomenon characterized by transient periods, usually lasting several seconds, in which attempted ambulation is halted. These events have been specifically described as “brief episodes during which patients find it impossible to generate effective forward stepping movements, in the absence of a cause other than parkinsonism or higher cortical deficits” [53]. Thus, FOG is not the result of muscle weakness, but is rather analogous to being “glued” to the floor. During FOG, while trying to move the feet to complete steps, the patient usually remains in the same place. Once the FOG event is overcome, the patient returns to moving at a normal pace until the next freezing episode develops [54], [55]. FOG is most commonly experienced during turning, step initiation and when the patient is faced with a special constraint such as a doorway, stress and distraction [54], [56]. Focused attention and sometimes external stimuli (cues) can help patients overcome FOG episodes. Because of its unpredictable nature, FOG often leads to falls [53]. Thus, FOG has notable clinical impact on PD patients owing to reduced mobility, loss of independence, recurrent falls, and subsequent physical injuries [57].

Most FoG episodes last less than 10 seconds, but as the disease progresses, the episodes occur more frequently and patients are less able to abort a freezing episode, leading to increased risk of falling. During the freezing episode, the person loses stability and has a higher risk of falling. Most falls of individuals with PD are intrinsic to the disease and may not be linked to the environment [52]. Due to the unpredictability of the episodes and the influence of attention and

sensory stimulus, it is often challenging to reproduce FOG episodes in regular clinical or research settings [58].

While the traditional dopaminergic medications effective in treating most of the motor symptoms of PD such as rigidity, bradykinesia and tremor, FoG episodes are notoriously resistant to levodopa, especially as FoG worsens with the progression of PD [59]. Recent studies have reported reduction in the number of FoG events for patients by using auditory [60], visual [61], and haptic feedback [62]. Thus, non-pharmacological interventions using external sensory feedback are a promising tool to reduce or prevent FoG episodes.

To better understand how these various feedback methods, affect FoG episodes that occur outside of a clinical setting, several wearable devices have been implemented. These devices can be used to monitor the patients outside clinical settings quantitatively and continuously [63]. Furthermore, these devices could also be used to provide external sensory feedback during the episode. Many of these devices contain one or more Inertial Measurement Units (IMU) mounted at different locations on the body, e.g., upper, or lower extremities, pelvis, or the back.

4.1 Related Work

To identify FoG episodes, wearable devices must be paired with different algorithms that process the sensor readings to identify the episode. To achieve this, the signals from the sensors are analyzed to identify characteristic features, which could be spatial [64]–[66], temporal [67], or in the frequency domain [68], [69]. After identifying these features, rules are set to recognize FoG. This process requires detailed processing and feature extractions from each sensor. While the addition of sensors might increase the reliability of the identification, it also increases the complexity of the algorithms.

Table 4 State-of-the-art methods to identify FoG using wearable sensors

Author	Sensor Location	Sensor Type	Algorithm	Sensitivity	Specificity	Precision	Accuracy
Capecci [68]	Waist	Acc	Threshold	87.5%	94.9%	69.5%	84.3%
Rezvanian [69]	Shin	Acc	Wavelet Transform	84.9%	81.0%	N/R	N/R
Ahlrichs [64]	Waist	Acc	Support Vector Machine	92.3%	100.0%	N/R	N/R
Martín [65]	Waist	Acc	Support Vector Machine	91.7%	87.4%	N/R	N/R
Tripolity [66]	8 sensors, full body	Acc, Gyro	Random Forests	81.9%	98.7%	96.1%	89.0%
Mazilu [67]	Chest, fingers	EKG, Skin	Threshold	76.2%	N/R	66.0%	N/R
El-Attar [70]	Shank, thigh, hip	IMU	ANN	100.0%	87.5%	88.9%	93.8%
Marcante [71]	Feet	Press, Acc	Rule based	96.0%	94.0%	N/R	N/R
Xia [72]	Shank, thigh, hip	Acc	ANN	69.3%	90.6%	N/R	N/R

Table 4 shows a summary of the state-of-the-art for identifying FoG using wearable devices. Capecci et al. [68] developed an algorithm that uses onboard sensors in a smartphone to detect the FoG events in 20 PD patients. The phone was attached to the waist by an elastic belt. The measured acceleration within a window of 2.5 seconds was used to calculate the Fast Fourier Transform (FFT) and identify its power spectrum. The complexity of the calculations was

minimized by only using vertical accelerations. To detect the FoG, a thresholding of the variables was used. The threshold was tuned for each subject to detect the maximum number of FoG events.

Ahlrichs et al. [64] and Martín et al. [65] used an accelerometer on the waist and a Support Vector Machine algorithm to detect the FoG. Both algorithms used the same dataset and calculated FFT and a variable window size to identify the optimal time window. Ahlrichs added a combination of thresholds to the features to improve the classification performance. To use the data from the accelerometers, the signals were resampled, filtered, and the FFT was calculated. This negatively impacts the prediction speed due to the computations involved.

Rezvanian et al. [69] used an accelerometer at the shin and Continuous Wavelet Transform (CWT) to identify FoG. A window of 2 seconds was used for the CWT and a threshold was set for each subject. The acceleration data was filtered and resampled. The prediction time was capped at 0.5 seconds, or 2Hz. Tripolity et al. [66] used six accelerometers and two gyroscopes. They tested four machine learning algorithms and used the entropy as the input feature. A window of one second was used with 0.5 seconds of overlap. They found that Random Forests gave the best performance on their dataset.

The above models require extensive data preprocessing for an optimal performance of identification. This has an impact on the speed of event identification and therefore limits the ability to deliver real-time feedback. Being able to identify the episodes faster would facilitate the delivery of real-time feedback.

4.1.1 Neural Networks for Freezing of Gait Identification

Artificial Neural Networks (ANN) are models that can automatically map an input to a class. These networks use supervised learning, i.e., each input in the training has a known true

output to automatically calculate weights that transform the input into the output. To learn the mapping, stochastic gradient descent, and backpropagation [44] are used to minimize a cost function. This property allows the network to analyze several different signals in a single step without increasing the network complexity. Furthermore, they can combine spatial and temporal data. Although the training of the ANN is computationally expensive, they can ultimately be compiled to map the signals rapidly without any preprocessing being required [12].

Lorenzi et al. [73] implemented an ANN to identify common behaviors of FoG. This included stopping during gait, short steps, and trunk fluctuations. These behaviors were only tested on healthy individuals but were not tested on PD patients. The authors used a shallow network of only two layers to minimize the computation time. They used the raw data from an accelerometer and only used fully-connected layers.

El-Attar et al [70] used a combination of Discrete Wavelet Transform (DWT) and ANNs to detect FoG. They used data from 10 patients with PD and a shallow network with two layers and 20 neurons to obtain a sensitivity of 100%, but they had to augment the data with frequency domain information identified separately from the dataset.

To avoid any preprocessing, different types of layers could be used to automatically encode information. Convolutional Neural Networks (CNN) use the convolution operator to find the kernel parameters automatically, reducing noise by encoding and decoding the data [27].

Recurrent Neural Networks (RNN) capture time dependencies in the data and generate sequence-to-sequence mapping [29]. RNN models use leaky units to help the network maintain its state, accumulate data over time, and forget the previous states when they are no longer relevant [27].

An ANN model which combines the signals recorded by an instrumented footwear to predict if a FoG episode will occur was designed. The model is capable of continuous predicting FoG at a high temporal resolution. We present the results of testing this model on data from 10 patients with PD and frequent FoG episodes.

4.2 Experiment Design

The training dataset contains data from 10 subjects with Parkinson's Disease (6 males and 4 females, with 10.5 ± 6.63 years of PD and a Hoehn and Yahr stage of 2.8±0.7) who exhibited FoG episodes during the recording. The participant characteristics are shown in Table 5. Each participant walked in multiple continuous laps on a 7-meter Zeno Walkway (Protokinetics, PA, USA) for 6 minutes. Once the participant reached the end of the walkway, they would turn around and walk back across the mat to where they began. This procedure was repeated for the duration of the recording. If the participant felt tired, they could rest between laps until they recovered. One video camera was placed at each end of the walkway and an investigator followed the subject as they walked with a third video camera focused on the participant's feet.

Table 5 Patients characteristics

Sub ID	Gender	Age [yrs.]	Weight [kg]	Height [m]	Reported FoG	Years of PD	H&Y stage
Sub001	Male	57	72	1.67	Yes	11	3
Sub002	Male	69	86	1.8	Yes	2	4
Sub003	Male	78	76	1.7	Yes	4	4
Sub004	Male	67	82	1.8	No	8	3
Sub006	Male	63	84	1.75	Yes	14	2
Sub007	Female	71	69	1.55	Yes	14	2
Sub008	Female	55	68	1.7	Yes	14	2
Sub009	Male	76	93	1.78	No	5	2

Sub010	Female	68	68	1.62	Yes	7	3
Sub011	Female	75	53	1.55	Yes	26	3

The subjects wore the DeepSole System over the duration of the experiment. The system collected signals from twelve channels: three pressure signals, three linear accelerations, three angular velocities, and three Euler angles. The pressure sensors are made with piezo resistive e-textiles cut to the shape of the insole. They are located under the phalanges, the metatarsals, and the calcaneus. The resistance of the fabric decreases when the applied force increases anywhere on the sensing area. By placing the sensors in the aforementioned locations, we can capture loading changes during the gait. The accelerations, angular velocity, and Euler angles are measured in the local IMU coordinate system. The sensor readings are recorded at 50Hz on an on-board microSD card and streamed through Wi-Fi using User Datagram Protocol (UDP) data packets.

The video cameras and the DeepSole System were synced to the Zeno Walkway time by using a custom circuit that turns on a light and broadcasts a UDP packet through the network at the start of the session. The light was in a place visible to all three video cameras and the DeepSole system recorded the time when the sync UDP was received. The Zeno Walkway was only used to synchronize the recording and standardize the length of the distance traveled per lap for each subject.

4.3 Gait Parameters

Ten gait parameters were chosen to analyse the differences between the laps where the subjects presented a FoG and where the FoG was not present. These parameters were obtained from the Zeno Walkway software (PKMAS). The strides used in this analysis are only the strides performed on the instrumented mat. Stride length (SL), stride width (SW), and step length (SpL)

were chosen to see the effects on the spatial characteristic of the gait [74]. For the temporal characteristics, stance time (SaT), swing time (SwT), step time (SpT), and stride time (ST) were chosen. For balance parameters, toe in/out angle (TA) and center of pressure distance (CD) during stance were chosen. The mean and standard deviation of these gait parameters are shown in Table \ref{tab:gait_pars}.

The progression vector is defined from the location of the heel strike from one side to the subsequent heel strike of the same side. The norm of this vector is the SL. SW is defined as the perpendicular distance from the progression vector to the heel strike of the opposite side. SpL is defined as the distance from the location of the heel strike to the heel strike of the opposite side, measured along the progression vector.

The TA is the angle between the direction of progression and the line connecting the heel and the toe of the foot. This parameter has an impact on the base of support and can affect the balance of the person. CD is the distance the center of pressure moves during the stance phase. This is a measure of how stable the person was while moving forward.

SaT is the duration that the corresponding foot is in contact with the ground, this is between heel strike and toe off. SwT is the duration between toe off to the subsequent heel strike of the same side, i.e., the period that the foot is not in contact with the floor. SpT is the time from heel strike until the heel strike of the other side. ST is the time from heel strike to heel strike of the same side, this also corresponds to SaT + SwT.

Table 6 Patients Gait Characteristics

	REG	FOG
Step Length (cm.)	54.0±12.5	47.3±10.5
Stride Length (cm.)	107.4±23.9	94.5±19.6
Stride Width (cm.)	8.3±4.4	8.0±4.4
Stance Time (sec.)	0.8±0.2	0.8±0.3
Swing Time (sec.)	0.4±0.2	0.4±0.1
Toe In/Out Angle (deg.)	5.0±23.0	9.7±8.7
COP Distance (cm.)	27.1±5.5	26.0±4.7
Step Time (sec.)	0.6±0.2	0.6±0.2
Stride Time (sec.)	1.1±0.3	1.2±0.3

4.4 Gait Parameters Statistical Analyses

The subjects walked a total of 323 laps on the walkway. From those, the subjects presented a FOG event while turning in 108 laps and did not presented a FOG event in 215 laps. A statistical study was done on all the gait parameters mentioned before to test if the gait of the subject was different a few strides before their motion was impaired.

For SL, SW, SpL, SwT, ST, TA, and CD data were normally distributed, as indicated by the Kolgomorov-Smirnov test and Q-Q plots. Thus, a repeated measurements ANOVA test was used to evaluate significant differences among the FOG laps and the non FOG laps. For SaT, SpT, and ST data were not normally distributed, as indicated by the Kolgomorov-Smirnov test and Q-Q plots. Thus, non-parametric statistical analyses were used. The Kruskal–Wallis test was used to evaluate significant differences among the FOG laps and the non FOG laps. Statistical significance was defined for *:$p<0.05$, and tests were run using statsmodels Python module [75]. For the normally distributed parameters, the F ratio and significance level (p-value) are presented for each variable. For the non-parametric test, the test statistic (χ^2) and significance level are shown.

For the spatial parameters, SpL ($F = 0.63$, $p = 0.45$) and SL ($F = 0.71$, $p = 0.42$) were not statistically different. But SW ($F = 8.50$, $p = 0.02$) was statistically smaller before the subject was affected by a FOG event. The box plot with the mean and inter-quartile information is shown in Figure 4.1.

As for the temporal parameters, neither SaT ($F = 0.01$, $p = 0.97$), SwT ($\chi^2(1) = 3.65$, $p = 0.09$), SpT ($F = .01$, $p = 0.92$), nor ST ($F = 0.01$, $p = 0.97$) were significantly different. The box plot with the mean and inter-quartile information is shown in Figure 4.2.

For the balance parameters, TA ($F = 8.68$, $p = 0.01$) was statistically larger and CD ($F = 9.45$, $p = 0.01$) was statistically smaller. The box plot with the mean and inter-quartile information is shown in Figure 4.3.

The statistical study shows that the gait of people who present FOG is different before they present the event. This is true even within small number of steps per lap (8.3±3.44 average steps per lap). This result allows us to do a more granular type of identification, where we can use a DeepSole sensors to predict the current state of the patient, i.e., if the patient is currently in a FOG state.

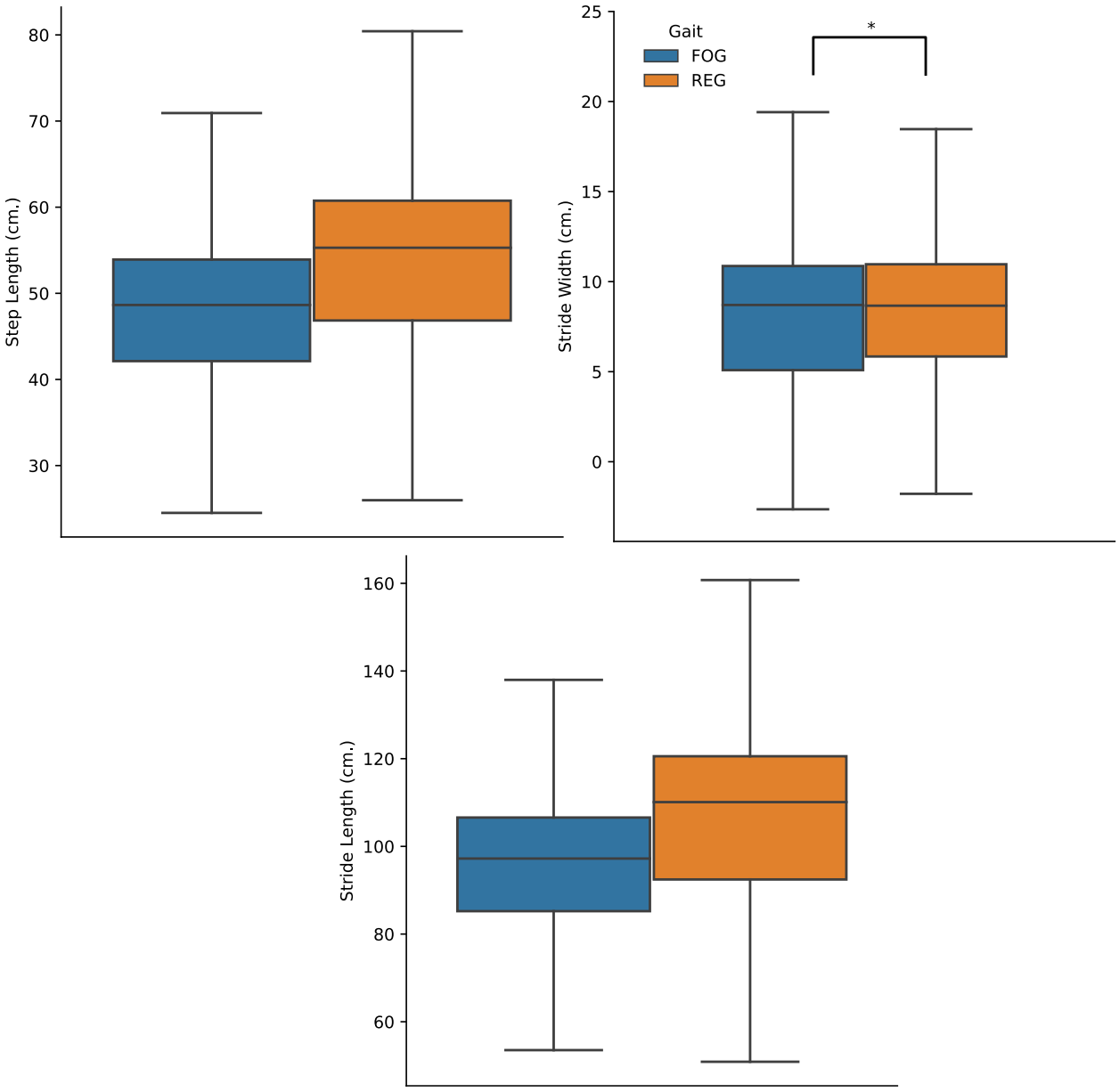

Figure 4.1 Box plots for the spatial parameters of the PD patients. Blue boxes are the mean of the laps where a FOG event was present, and orange boxes represent the laps where no FOG events were registered. Statistical significance is show with *: $p < 0.05$.

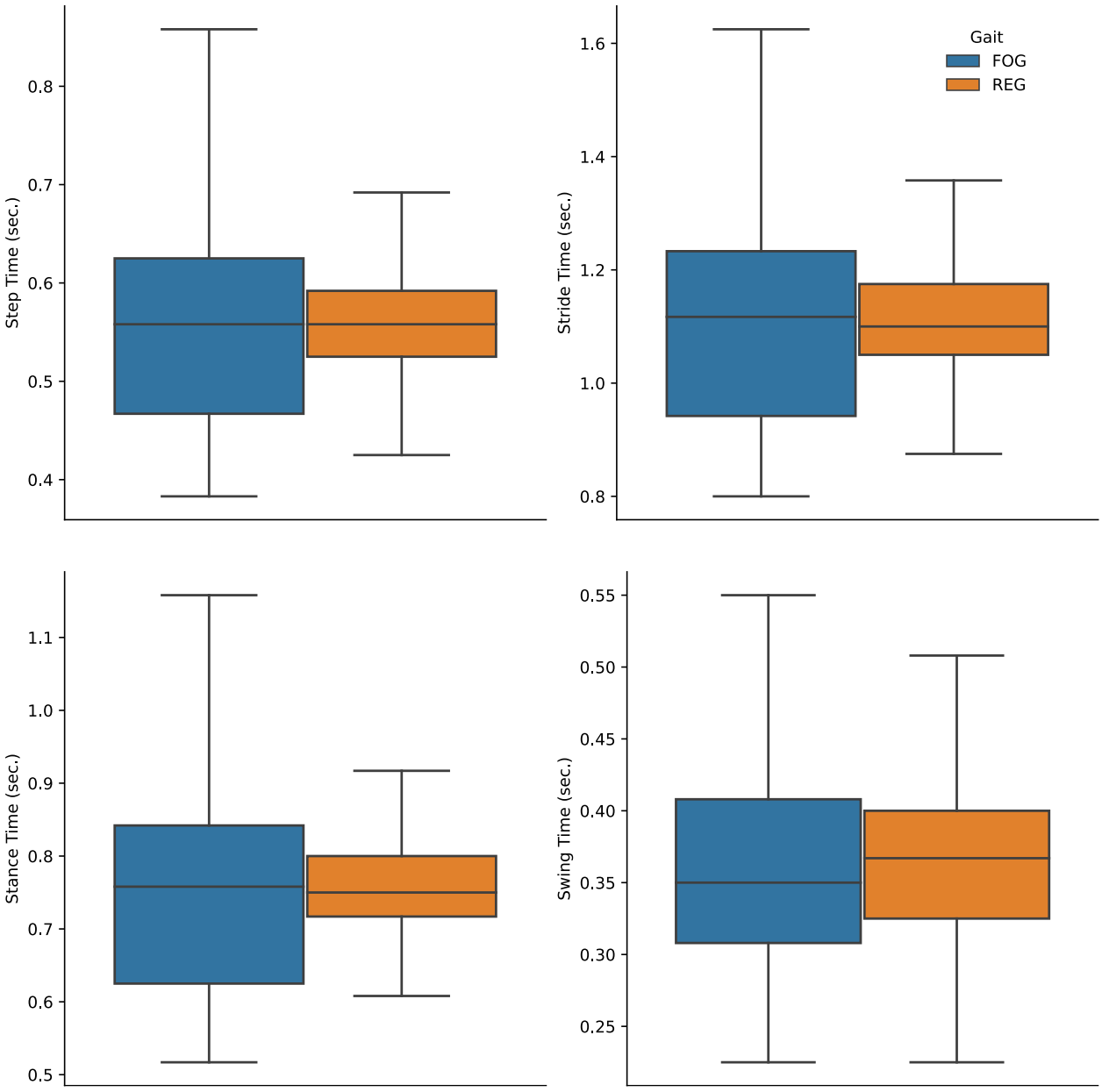

Figure 4.2 Box plots for the temporal parameters of the PD patients. Blue boxes are the mean of the laps where a FOG event was present, and orange boxes represent the laps where no FOG events were registered. Statistical significance is show with *: $p < 0.05$.

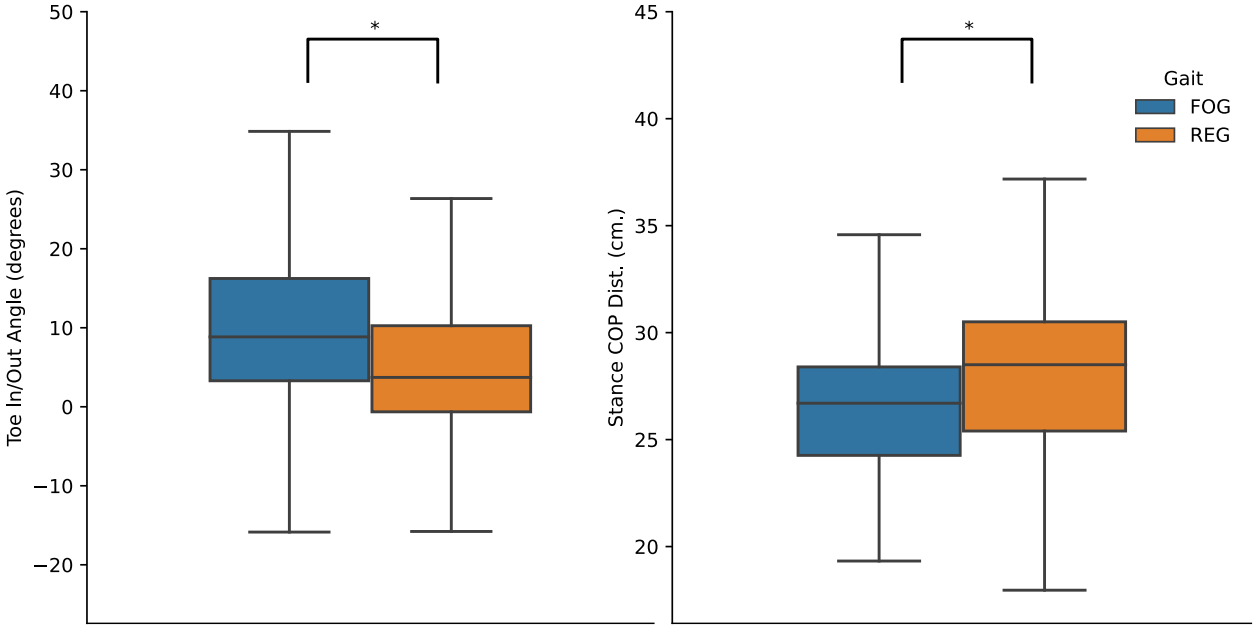

Figure 4.3 Box plots for the balance parameters of the PD patients. Blue boxes are the mean of the laps where a FOG event was present, and orange boxes represent the laps where no FOG events were registered. Statistical significance is show with *: p < 0.05.

4.5 Neural Network

4.5.1 Sensor Segmentation

Considering the results from the statistical analysis performed in the previous section, we have confirmed that the gait of the patients is different in the laps where a FOG event occurred from those where the episode did not occur. We can use this property to map the signal from the DeepSole sensors to the current state of the gait (freezing or regular gait). To achieve this, we need to segment the data into windows.

For each time *t*, the Deepsole System records twelve sensor values for both the left and right foot. To identify the FoG, a window of 0.5 seconds was used to predict if the wearer will have a FoG event at time $t+dt$. The 0.5 second window was chosen because it represents approximately half a cycle. This amount has been found to be enough to represent the time history

of a gait event [76]. Furthermore, by using this window size, the neural network can be computed at the same rate as the DeepSole sampling rate.

Given that the Deepsole records data at 50Hz, at each time *t*, we created two matrices of size 25x12. Each column represents a sensor signal, and the row number corresponds to the time. To use with the neural network, the matrices from the right and left shoes are stacked into a 3D tensor of shape 25x2x12. The last row is the latest reading from the sensors and the first is the reading at *t-49dt*.

4.5.2 Identifying the Freezing of Gait Events

The video recordings were used to identify the FoG events. A clinical expert coded the videos to identify when the FoG episode started and when it stopped. The video was coded with a resolution of 1 second. This code was transformed into a continuous binary signal super sampled to the DeepSole System time, Eq. (7). In this signal, a value of 0 represents regular gait (REG) and a value of 1 represents FoG.

$$y_T(t) = \begin{cases} 0\ REG \\ 1\ FoG \end{cases} \tag{12}$$

Equation (7) was used as the ground truth for the supervised learning of the ANN by pairing each value of $y_T(t)$ with the corresponding sensor reading from the DeepSole. The video coding includes the continuous walking and the turning at the end of the walkway.

4.5.3 Architecture

To predict if the wearer has a FoG episode given the sensor signals recorded from the DeepSole System, an ANN was created. We combined 2D CNN to encode-decode the signals and RNN to learn the temporal relation in the sensor readings [49]. Dropout of 50% was used throughout the network [50]. Figure 4.4 shows a graphical schematic of the network. To train the network, the dataset was used as supervised learning, where each input has a corresponding truth output. During training, the initial 75% of the data recorded was used for training and the last 25% was used for evaluation.

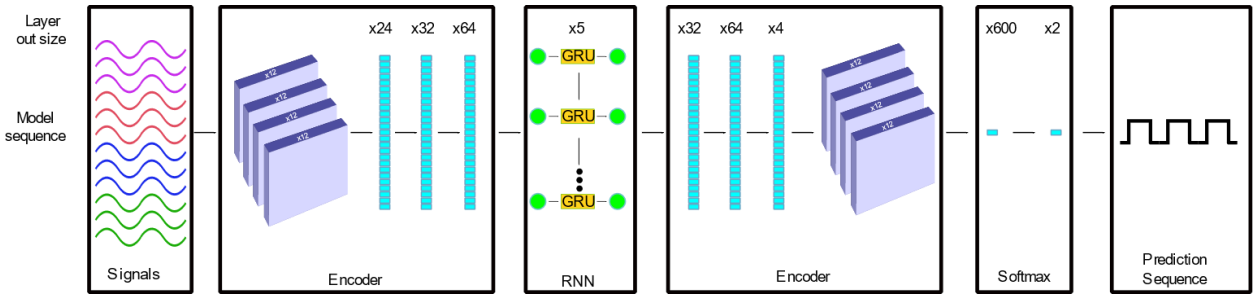

Figure 4.4 Graphical overview of the neural network with an Encoder-Decoder RNN architecture. The model maps the 12 signals collected by the DeepSole system into the predicted FoG episode. A value of 0 corresponds to regular gait and a value of 1 corresponds freezing.

The model starts with an encoder with four 2D CNN layers. All dimensions of the inputs are kept constant throughout the convolution layers by setting the number of filters to 12 and the paddings to the same number. The rectified linear unit (ReLU) function was used at each layer. The kernel size was 30 for layer one, 20 for layer two, 10 for layer three, and 5 for layer four.

After the convolution, the outputs from the CNN were reshaped from 25*x*2*x*12 to 25*x*24 and passed through two fully-connected layers with 32 and 64 units respectively, with a ReLU activation.

The outputs from the fully-connected layers were fed into a recurrent layer. The recurrent layer contains 5 Gated Recurrent Unit (GRU) cells [48] with a ReLU activation. After the recurrent layers, three fully-connected layers were used with 32, 64, and 4 neurons, respectively.

The outputs were then reshaped back into 25*x*2*x*2 and passed through a 2D CNN decoder of four layers. Again, the dimensions were kept constant within the convolutions and a kernel size of 30, 20, 10, and 5 were used respectively for the layers.

Finally, the output was flattened and passed to a fully-connected layer with 2 neurons and a SoftMax activation to create a probability vector of FoG. The class with the highest probability was chosen as the final output $y_P(t)$.

The model was trained for 200 epochs. For each window presented, the corresponding value of $y_T(t)$ was presented. The loss used was sparse categorical crossentropy. The loss was minimized by applying the Adam optimizer [77]. A learning rate of $1e^{-4}$ was used, and 50% dropout was used throughout the models to avoid over-fitting [50].

4.6 Metrics

The binary FoG function $y_T(t)$ (ground truth) was compared against the output from the ANN $y_P(t)$ (predicted event) to evaluate the performance of the ANN. The number of correctly identified episodes of FoG was labeled as True Positives (TP) and the number of incorrectly FoG identified was labeled as False Positives (FP).

Similarly, for REG events, the correctly identified events were labeled as True Negatives (TN) and the misidentified were labeled as False Negatives (FN). Four parameters were evaluated [78] to assess the performance of the networks:

1) *Sensitivity*: The proportion of FoG samples correctly identified in y_P divided by the total FoG samples in y_T.
2) *Specificity*: The number of REG samples correctly identified in y_P divided by the total REG samples in y_T.
3) *Precision*: The number of FOG samples correctly identified in y_P with respect to the total number FOG samples identified by y_P.
4) *Accuracy*: The percentage accuracy between the ground truth and the predicted output was calculated as the proportion of correct prediction to the total number of samples.

For all the calculations, y_T and y_P were used at the original 50Hz that the DeepSole recorded the data. This was done because the goal of the model is to identify the FoG episodes as soon as possible in real-time.

4.7 Results

Data was aggregated and prediction metrics were calculated. The data used was the last 25% of the data recorded for each subject, as this data was not used during training. Table 7 contains a summary of the results. Figure 4.5 shows bar plots of the metrics.

The model sensitivity was 96.0±2.5% FoG events, but 11.6±6.9% of the FoG events were mislabeled (False Positives). The precision was 89.5±5.9%. This represents the ability of the model to identify the FoG samples. The model was able to identify the FoG episodes that occurred during

straight walking and during turning with high sensitivity and precision. This was true for all subjects in the dataset. The presented model outperforms state-of-the-art methods for precision. For sensitivity, only El-Attar [70] has a higher rate, but they use a higher number of sensors.

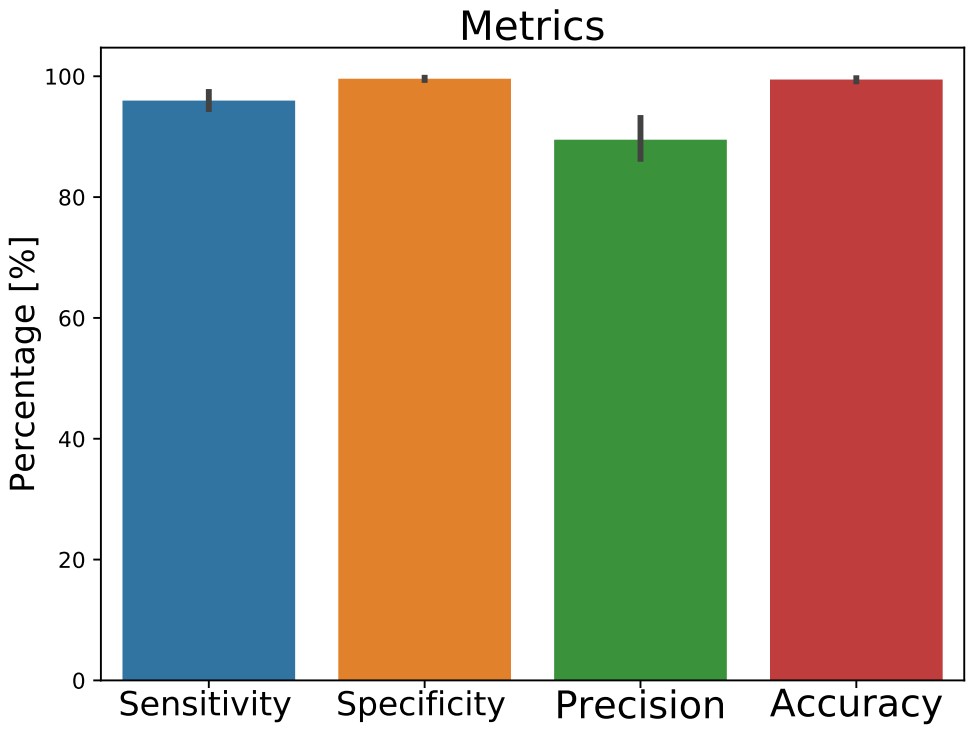

Figure 4.5 Bar plot of the four main metrics used to evaluate the model. The height is the average among subjects and the whiskers are ± one standard deviation. The blue bar is the Sensitivity, the orange is Specificity, the green is Precision, and the red is Accuracy

For the REG events, the model specificity was 99.6±0.3%, but 0.2±0.2% were incorrectly identified (False Negatives). This shows that the model excels at not identifying regular gait as FoG. This is especially useful at the edges of the walkway when the subject is turning. During turning, the subject stops and turns, but the model correctly identifies this REG without information about the frequency domain. This metric is also better than the current state-of-the-art, almost matching the 100% specificity reported by Ahlrichs et al [64].

Table 7 Metric summary

Metric	Mean ± SD
Sensitivity	96.0±2.5%
Specificity	99.6±0.3%
Precision	89.5±5.9%
Accuracy	99.5±0.4%
False Positives	11.6±6.9%
False Negatives	0.2±0.2%

The overall accuracy of the prediction was 99.5±0.4% for the complete recording of all 10 subjects. This shows that the model behaves well for both FoG and REG events, even if the gaits characteristics differed between individuals. Furthermore, the small standard deviation of all the metrics shows that the model can predict the FoG events of all patients equally well, despite subjects having different physiological characteristics and different stages of PD.

4.8 Conclusion

The proposed algorithm can identify the FoG events with high accuracy at a high frequency of 50Hz using the signals from the DeepSole system. It uses a window of 0.5 seconds but generates a prediction at the original 50 Hz. This property allows the algorithm to identify the episode within one sampling frequency of the DeepSole System, i.e., 20 milliseconds. This is tested with 10 PD patients that suffered from FoG. The algorithm can accurately identify the FoG events with a small

number of false predictions without requiring manual calibration, unlike thresholding algorithms. For the presented model, the ground truth was coded with one second resolution. This was deemed sufficient, as all freezing episodes last longer than this period. Although, this resolution could be improved to better identify the onset on the episode.

The combination of the ANN model with the DeepSole System allows us to have a setup that is portable, comfortable to wear, minimally invasive and capable of timely identification of FoG episodes. This is an important feature, as many patients find it hard to wear systems that require multiple sensors placed on different areas of the body. As shown in Table 4, different authors use different numbers of sensors at several segments of the body. The DeepSole system provides a platform where all sensors are contained within a pair of shoes, simplifying both the setup and the comfort.

The model outperforms the current state-of-the-art in the evaluated metrics. Further studies can focus on the effects of each of the sensors on the network performance. The presented model uses the raw data from all 24 sensors placed at the foot of the wearer without any filtering or preprocessing. This was chosen because ANN can be used as a general regressor between workspaces without requiring engineered features on the data to be found. This is thanks to their ability to detect possible interactions between the input sensors [79]. Therefore, all the sensors can be used without having to create a complex rule set.

By using convolutional and recurrent layers, the algorithm can avoid frequency domain transformations like Fast Fourier Transforms [80]. This property contributes to the speed of the prediction being the same as the sampling frequency. To further improve the speed of prediction, different combinations of layers and sensors included in the input could be changed. This would also give insights on the main contributor to the performance of the network.

The dataset collected showed that the gait of PD patients is highly variable. During the stride on the onset of the event, the patients are less stable. With a statistical change to their stride width, toe in/out angle, and center of pressure distance during stance phase. Although further analysis should be done to understand how many strides prior to the events are different to the regular gait. This result also shows that the changes can be different depending on the patient. For example, the study presented by Nieuwboer et al. [81] found differences in the stride length and cadence, but in our dataset these parameters where not statistically different. Moreover, spatiotemporal parameters of gait in PD patients ameliorate after vibration and in particular in the stride length and cadence, after the erector spine muscle vibration [82]. Step synchronized haptic feedback has been shown to reduce the number of FoG episodes on case studies [7]. This could be because PD patients unable to properly control their postural orientation based on the available sensory information [83] and haptic feedback can enhance the motor sensing feedback, thus improving their postural control [84]. To minimize the effect of this inter-subject variation, we used the raw sensor data from the DeepSole. These signals can capture different spatiotemporal gait characteristics, so the identification should be more robust than with abstract gait parameters.

The wireless capability of the DeepSole system would allow us to implement the algorithm in real-time at the same sampling frequency as the data acquisition. Although the 50 Hz could not be achieved on an embedded computer, a simulation was made by sending the real-time session recording to a desktop computer. On a desktop computer with a Nvidia 2080 video card, the model could be run at a frequency of 50Hz. This needs to be tested further outside simulation. In a real environment, the identification rate could be affected by unknown variables, like the network latency and loss of data packets. By using real-time identification, auditory or haptic feedback could be provided as needed to the patient. The high frequency detection of 50 Hz could be used

to provide sensory feedback to help patients with FoG. This would have a positive impact on their daily living.

Chapter 5: Gait Phase Timed Vibration

Gait training has shown positive results in the treatment of gait deficits in different populations groups, such as post stroke survivors [85] and those with knee osteoarthritis [86]. Gait feedback can be discrete, based on gait event detection [87], or continuous, based on errors from a specified trajectory [88]. For both situations, it is vital to track gait events and phase during the gait cycle.

Vibratory feedback has been used in a wide range of studies in various populations. It is most used as a cueing system. For example, Crea et al. [89] used an instrumented insole and 3 vibratory devices mounted at the abdomen to provide feedback for gait symmetry on patients with lower limb amputation. The vibrators activated at heel strike, mid foot, and toe off to signal the subject about state of the prosthesis. In the study they showed that the subjects were able to improve their symmetry without any evidence of an increased cognitive burden.

Ma et al. [90] used a vibrator mounted at the wrist of patients with stroke to foot inversion and mid-stance foot-floor contact. During the experiment, the patients wore an instrumented insole on their paretic side. When the loading was asymmetric, the vibrator was turned on to cue the subject to even their loading. The subjects were able to significantly reduce the foot inversion, bringing the loading levels of the paretic side to similar values as their non-paretic side.

Afzal et al. [91] used instrumented insoles and vibrator mounted at the calf to study the ability of people to identify different duration of vibratory feedback while walking. In their study they found that dominant and non-dominant sides are good at identifying the duration of the vibratory feedback. Also, they found that the stance symmetry ratio changed when the cues were

provided, although this was not the goal of the study. The experiment was done on healthy individuals and the change in symmetry ratio was not analyzed in detail.

Later on, Afzal et al. [92] used the system on stroke survivors to improve the temporal symmetry ratio between the paretic and the non-paretic legs. Four different strategies were tested, this were proportionally increasing or decreasing the vibration time and intensity. They used FSR sensors and thresholding to identify the heel strike events. The vibratory feedback was a constant duration or intensity depending on the symmetry ratio recorded during a session without any feedback. In this study, they found that all strategies improved the temporal symmetry ratio, but there was no significant difference between the vibration strategies. This study shows the promise of using vibratory feedback to improve symmetry on patients who suffered a stroke. But given that a thresholding algorithm was used it requires per subject calibration.

To test if ANN could be used as a real-time sensor for human motion for gait cycle phase identification, the algorithm presented in Chapter 2 was implemented for real-time phase prediction. By using the properties of sequence-to-sequence mapping, the model can map raw sensor data to abstract motion characteristics at a frequency 46 Hz. It has been shown that during walking, most frequencies of human movement are under 6 Hz [16]. Thus, this processing speed would be enough to capture the kinematics and kinetics during walking.

Using the phase prediction, heel strikes (HS) were identified as the instance when the signal changes from swing to stance. When a HS was identified, vibratory feedback was provided to the wearer. The vibration was given in the sole of the non-dominant side. The duration of the vibration was 125% of the subject's baseline stance time.

The hypothesis for this experiment is that by providing vibratory feedback only on the non-dominant side, the subject will walk asymmetrically. If the hypothesis is true, this protocol could

be later implemented with populations that present asymmetric gait, like those with CP or stroke survivors.

5.1 Methods

A total of 9 subjects participated in the experiment. All subjects were naïve to the experiment and agreed to participate by signing a consent form. The protocol was reviewed and approved by the Columbia University Institutional Review Board. The experiment consisted of 16 minutes of walking divided into 3 sessions, Figure 5.1 shows an overview of the protocol. During the experiment, data was collected by both the DeepSole system and the Zeno walkway.

Figure 5.1 Overview of the gait phased timed vibration protocol. The experiment had 3 session where the subjects walked back and forward on the Zeno Walkway while wearing the DeepSole system

For the baseline session, the subjects walked at a self-selected speed for 3 minutes. The subjects were asked to walk naturally. This session was used to calculate the baseline values for the stance phase duration of each subject. For this session, the DeepSole system was used only for data collection and no feedback was given to the subject.

The second session consisted of 10 minutes of waking. During this time, the DeepSole system streamed the sensor data to a computer, where the phase prediction was calculated. When

a HS was detected, the vibratory motors were turned on the non-dominant side of the subject. The subject was instructed to maintain contact with the ground if the vibration was on. For the dominant side, the subject was instructed to maintain their regular gait. Thus, creating temporal asymmetry.

The last session was 3 minutes long. For this session, there was no vibratory feedback and the DeepSole system was used only for data collection. During the session, the subject walked at self-selected speed again.

5.1.1 Metrics

The prediction of the implemented model was compared against the recording from the Zeno Walkway to evaluate the performance of the ANN. The number of correctly identified HS was labeled as True Positives (TP) and the number of incorrectly HS identified was labeled as False Positives (FP).

Similarly, the correctly identified not HS events were labeled as True Negatives (TN) and the misidentified were labeled as False Negatives (FN). Five parameters were evaluated [78] to assess the performance of the networks:

1) *HS Sensitivity*:

$$\text{Sensitivity} = \frac{TP}{(TP + FN)} \, x \, 100 \tag{7}$$

2) *HS Specificity*:

$$\text{Specificity} = \frac{TN}{(TN\ +\ FP)}\ x\ 100 \tag{8}$$

3) *HS Precision*:

$$\text{Precision} = \frac{TP}{(TP\ +\ FP)}\ x\ 100 \tag{9}$$

4) *HS Accuracy*:

$$\text{Accuracy} = \frac{(TP\ + TN)}{(TP\ + FP\ + TN\ +\ FN)}\ x\ 100 \tag{10}$$

5) Model Prediction Accuracy:

$$\text{Model Accuracy} = \frac{Predicted\ Phase\ ==\ True\ Phase}{True\ Phase}\ x\ 100 \tag{11}$$

Data of the model accuracy were not normally distributed, as indicated by the Kolgomorov-Smirnov test and Q-Q plots. Thus, non-parametric statistical analyses were used. The Friedman test was used to evaluate significant differences among the 5 methods of interest. In the case of significance, Wilcoxon signed-rank tests were carried out as post-hoc testing using Bonferroni correction for the number of comparisons. Statistical significance was defined for *: $p < 0.05$, and tests were run using IBM SPSS Statistics 26.

5.1.2 Gait Parameters

To see the effects of the vibration feedback on the gait of the subjects, four gait parameters were chosen. Stride length (SL) and stride width (SW) were chosen to see the effects on the spatial characteristic of the gait [74]. For the temporal characteristics, stance time (ST) and swing time (WT) were chosen. SL is defined as the norm of the vector created from the location of the heel strike from one side to the next heel strike of the same side. This vector corresponds to that forward walking direction. Stride width is defined as the perpendicular distance from the walking direction vector to the heel strike of the opposite side. Stance time is the duration that the corresponding foot is in contact with the ground, this is between heel strike and toe off. Swing time is the duration between toe off to the subsequent heel strike of the same side, i.e., the period that the foot is not in contact with the floor. Spatial parameters are shown in Figure 5.2 and temporal are shown in Figure 2.1.

Data for the gait parameters were normally distributed, as indicated by the Kolgomorov-Smirnov test and Q-Q plots. Thus, 2-way repeated measurement ANOVA (rmANOVA) statistical analyses were used. The rmANOVA test was used to evaluate significant differences among the sessions and side and their interaction factor. In the case of significance, pairwise comparison tests were carried out as post-hoc testing using Bonferroni correction for the number of comparisons. Statistical significance was defined for *: $p < 0.05$, **: $p < 0.01$, and tests were run using IBM SPSS Statistics 26.

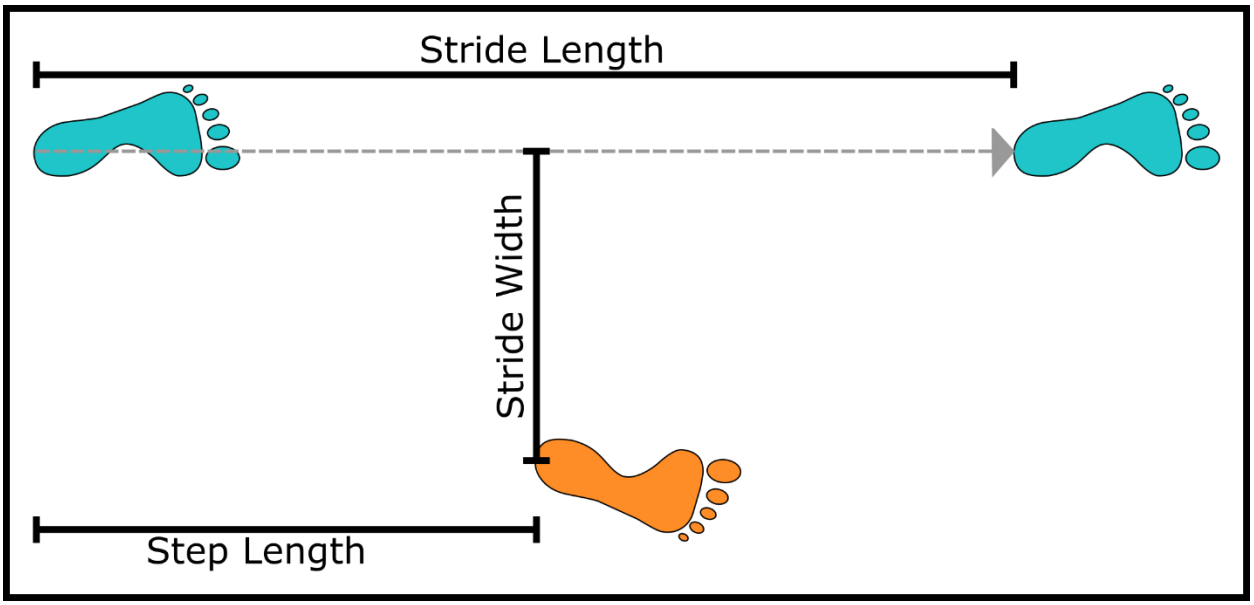

Figure 5.2 Shows how stride length, stride width, and step length are measured. Blue footprints are from the left side and orange are from the right. The gray arrow is the walking direction. The black lines are the different measurements.

5.2 Results

The predicted signal and HS values were recorded in real-time by the computer running the model. This warranties that the values compared are the same as those calculated during the experiment.

The data shows that the model prediction accuracy is above 90% for all three session. With values (mean ± sd) of 91.3±15.3% for the baseline, 91.0 ± 6.0 % for the training session, and 94.3 ± 3.8 % for the post-training session. This is shown in Figure 5.3. Although, the Friedman (χ (2) = 8.0, p = 0.018) test showed that baseline session was statistically different to the train session (z = 2.828, p = 0.014).

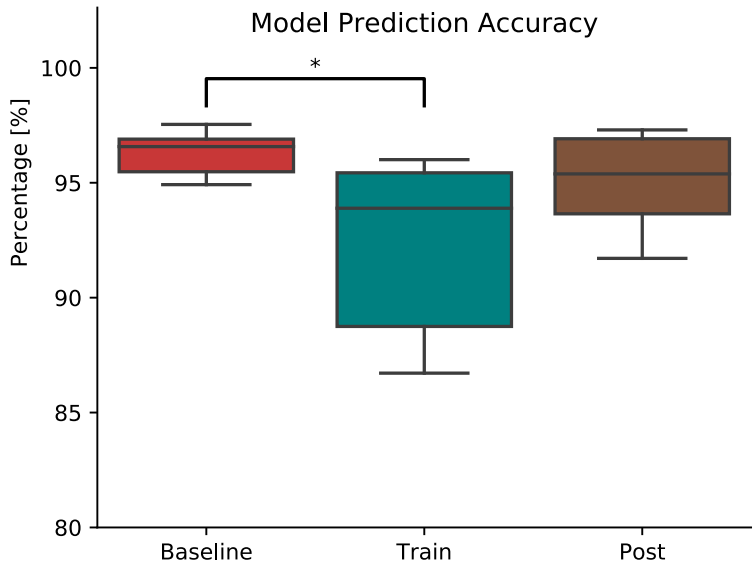

Figure 5.3 Box plot of the model prediction accuracy per session. The horizontal axis is the session, and the vertical axis is the accuracy in percentage. The lines on top of the boxes shows statistically significant differences between the session.

For the HS metrics, only the training session was used, this is because feedback was only provided during this session. Figure 5.4 show a bar graph with the metric values for both dominant and non-dominant sides.

The sensitivity for the dominant side was 78.5 ± 21.9 %, the specificity was 99.6 ± 0.3 %, the precision was 71.5 ± 18.2 %, and the accuracy 99.3 ± 0.7 %.

For the non-dominant side, the sensitivity was 73.2 ± 23.3 %, the specificity was 99.6 ± 0.2 %, the precision was 73.0 ± 15.2 %, and the accuracy was 99.3 ± 0.7 %.

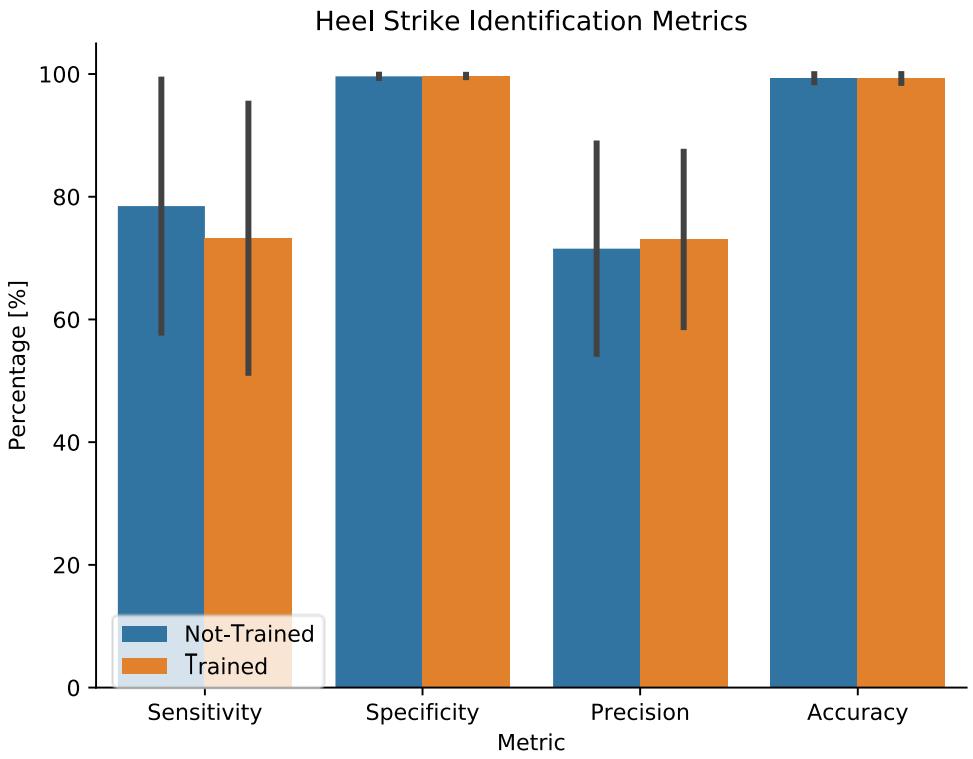

Figure 5.4 Bar plots showing the heel strike identification metrics values. The height of the bar shows the mean value, and the whiskers size corresponds to ± sd

The Friedman test on the HS metrics showed that there is no statistical difference between the model prediction between dominant and non-dominant. This means that the prediction is similar on both left and right side during the training session. This is true for all four metrics.

During the training session, the subjects had an asymmetric gait but only on the temporal parameters. For the spatial parameters, the subjects kept their symmetry across all session. The graphical representation of the gait parameters and symmetry is shown in Figure 5.5. The numerical values of the parameters are shown in Table 8, the values shown are represented by mean ± standard deviation.

Table 8 Gait Parameters per Session

	Parameter	Baseline		Train		Post	
		Not Trained	Trained	Not Trained	Trained	Not Trained	Trained
Spatial	Stride Length (cm.)	136.6 ± 15.9	136.7 ± 15.9	123.5 ± 14.0	123.5 ± 14.0	127.7 ± 14.2	127.9 ± 14.3
	Stride Width (cm.)	10.4 ± 2.5	10.2 ± 2.5	12.1 ± 3.2	12.1 ± 3.2	10.2 ± 3.0	10.3 ± 3.0
Temporal	Stance Time (sec.)	0.7 ± 0.1	0.7 ± 0.0	1.2 ± 0.2	1.4 ± 0.2	0.8 ± 0.1	0.8 ± 0.1
	Swing Time (sec.)	0.3 ± 0.0	0.4 ± 0.0	0.8 ± 0.2	0.5 ± 0.1	0.4 ± 0.1	0.4 ± 0.1

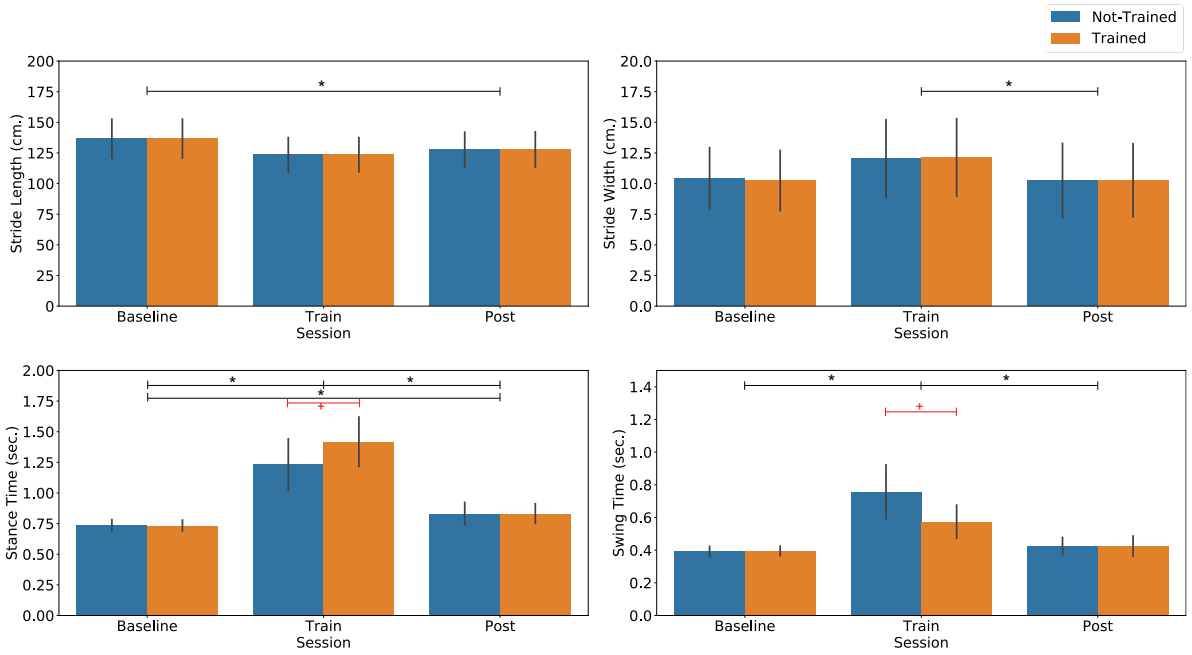

Figure 5.5 Gait parameters aggregated by session. For all plots, the horizontal axis is the session, and the vertical axis is the value of the parameter in its corresponding units. The blue bars correspond to the side without feedback, and the orange bars are the side with the vibratory feedback. Statistical difference between sessions is shown with black lines and * symbol. Interaction factor between the session and the side are shown with red lines and the + symbol.

5.3 Discussion

The model performance is sufficient for all sessions as the average performance is above 90%. Although there is a significant difference between the baseline session and the training session, this is since the subjects are actively modifying their gait during the session. Furthermore, the statistical test on the HS metrics between the sides showed that there is no difference between the left and right sides within the same session. This is true even during the training session, where the subjects walked asymmetrically.

As for the gait characteristics, the subjects walked symmetrically during the baseline and post sessions. This was expected as all subjects were normally developed adults without any pathology. During the training session, feedback was provided to modify the subject's stance time. In this session, the subject's SL was different between baseline and post; and the SW was different between training session and post session. Despite this difference, there was no interaction factor between the session and the side. This means that throughout all sessions their spatial parameters (SL and SW) were symmetrical.

As for the temporal parameters, ST was statistically different between all sessions. ST was longest during training, then post and the smallest were during baseline. For WT, training session was statistically longer than both baseline and post, but no difference was found between baseline and post. For both temporal parameters measured and interaction factor was found between side and session, as shown in Figure 5.5 this interaction comes from the asymmetry during the training session.

The results show that subjects were able to modify their gait during training based on the haptic feedback. Although the ST for both dominant and non-dominant side increased, the subjects walked asymmetrically with an average ratio of 1.16 ± 0.15. The ratio of the gait parameters is

shown in Table 9. This discrepancy could come from either the model or the subject reaction to the feedback. Given that the performance of the model, shown by the metrics, are all above 90%. We can safely assume that the increase time in ST comes from the subject reaction to the vibratory feedback. It has been shown in literature [93] that joint movement in response to vibration can take from 0.5s up to 2s. This reaction time depends greatly on the subject's ability to create a memory motor trace of the cyclic movement. Furthermore, given that walking is a bilateral activity, modifying one side has an impact on the other side as well.

Table 9 Symmetry Ratio for Temporal and Spatial Gait Parameters

	Parameter	Baseline	Train	Post
Spatial	Stride Length (cm.)	1.00 ± 0.00	1.00 ± 0.00	1.00 ± 0.00
	Stride Width (cm.)	0.98 ± 0.02	1.01 ± 0.02	1.01 ± 0.04
Temporal	Stance Time (sec.)	0.99 ± 0.01	1.16 ± 0.15	0.99 ± 0.04
	Swing Time (sec.)	1.00 ± 0.03	0.74 ± 0.14	1.01 ± 0.06

5.4 Conclusion

The algorithm was tested online with nine novel subjects. Haptic feedback was provided to the subjects to increase the dominant side stance time. The subjects were able to modify their gait but there was an intrinsic reaction time to the vibratory feedback. This reaction time slowed down the gait of the subjects, but the asymmetry was achieved during the training session.

The effect of the reaction time could be counteracted by simply shortening the duration of the desired ST time by a constant value. However, the inter-subject variability would still be

present as the subjects always have a reaction time to haptic feedback. To reduce this effect, the haptic feedback could be modified from a constant vibration to a variable vibration that reduces intensity as the end of the stance phase approaches or by pairing the haptic feedback to audiovisual feedback. These strategies could help the subject create a motor memory of the desired timing, hence reducing the reaction time.

The model presented can classify the phases of gait using the raw sensor data collected by the DeepSole system. The algorithm has consistent performance even when tested with novel subjects, maintaining over 90% accuracy running at a frequency of 50 Hz. Using a CNN encoder-decoder and an RNN, the system can map the sensors to gait phases without the need of pre-processing or post-processing.

Pairing this algorithm with the DeepSole system transforms the system into a high-level sensor that provides real-time status of the gait of the user. This capability could be paired with other devices, like leg exoskeletons, to provide open-loop feedback to the user.

Chapter 6: Timed Muscle Vibration

Human movement is complex as even single motions require coordination of several muscle groups. Furthermore, the motion needs a closed-loop control that ensures its correct execution. This loop control requires a good sense of position and movement of all the parts of the body, also known as kinesthesia and proprioception [94].

Proprioception relies on mechanosensors, also known as proprioceptors, distributed throughout the body [95]. During movement, the mechanosensors register the changes in the tissue in motion. This includes muscle length and tension, deformation of tissue like tendons, joint capsules, ligaments, and skin [96]. The information from the proprioceptors is constantly being received by the central nervous system [97].

Muscle spindles are used to sense the state of the muscle. These receptors are located in parallel with the muscle fibers and signal on length changes. Studies have found that the sense of position and the sense of motion is processed separately in the central nervous system [98]. The muscle spindles provide two information channels that fire at different rates when the muscle is being stretch or held under load [99]. The signal from the spindles changes depending on the muscle's previous history of length and contraction changes [100].

Although spindles are the main component of the sensors. Golgi tendons and skin receptors also contribute to the proprioception [101], [102]. The tendons are in series to the muscle and can detect the tension when a load is applied. When the muscle activates, there is an initial peak followed by a plateau. Their amplitude depends on the rate of change in the tension and the absolute tension value [103].

When the muscles and tendons are subjected to continuous vibration, the muscle spindles give the illusion of limb movement. This was demonstrated by Goodwin et al [104] by providing vibration at the elbow level to subjects while blindfolded. The vibration was applied only to one side, and the subjects were asked to track the position with their other arm. The experimenters reported that there was a lag in the arm tracking and a persistent error. Although, when the vibration is presented both at the agonist and antagonist muscle groups, it does not create the illusion of movement [105].

Furthermore, vibratory stimuli have different effect on muscles that are relaxed and those that are contracted. For example, high-frequency vibratory feedback can enhance movement speed by increasing preparatory beta desynchronization and placing the motor cortex in a "ready- to-move" state. This is because the vibration can decouple the tension and length information [101].

Macerollo et al. [106] measured EEG in a sample of healthy subjects before, during, and after peripheral vibration while subjects were at rest. The data revealed a significant decrease in beta power (15–30 Hz) over the contralateral sensorimotor cortex at the onset and offset of 80 Hz vibration. This vibration can modulate the uncertainty of the proprioceptive afferent signal, improving motor performance by allowing for top-down proprioceptive predictions [84].

In quiet standing, a vibration on the tibial anterior elicits a forward body tilt, whereas vibrations of the hamstring and triceps surae elicits a backward trunk. In treadmill locomotion, hamstring vibrations produce forward stepping [107]. Several muscles have been studied and it has been shown that the local vibratory feedback has a significant effect on the area where the vibration is applied [108] during locomotion.

During treadmill walking when a constant vibration is applied to hamstrings, subjects significantly increase their walking velocity and cadence [109]. Furthermore, when the vibration

is only applied to one side, the subjects balance metrics are affected [110], i.e., the subjects are less stable.

Due to the inherit complexity of continuous gait tracking, gait timed vibration has not been adequately studied. Most of the examples present in literature use specific events like heel strike to time the vibration. Duclos et al. [111] provided vibratory feedback at the triceps surae during stance phase but found no statistical difference in the spatiotemporal parameters of the gait. While Roden-Reynolds et al. [112] provided vibration to the gluteus medius during the swing phase. This strategy resulted in a wider stride width when the vibration was present. These studies used gait events to provide feedback, but complex synchronized feedback to the muscles during walking has not been studied.

The accurate prediction of the current gait cycle percentage opens the door to provide complex synchronized feedback to individuals. Furthermore, using the modular design of the DeepSole, we can easily expand the system functionality and add more than six vibrator motors. This upgrade allows us to provide continuous haptic feedback throughout the gait cycle.

We hypothesize that gait cycle timed vibration on several muscle groups when they are used during walking will modify the cadence and velocity of subjects, by exciting the muscles spindles.

6.1 Methods

A total of 7 subjects participated in the experiment. All subjects were naïve to the experiment and agreed to participate by signing a consent form. The protocol was reviewed and approved by the Columbia University Institutional Review Board. The experiment consisted of 16

minutes of walking divided into 3 sessions, Figure 6.1 shows an overview of the protocol. During the experiment, data was collected by both the DeepSole system and the Zeno walkway.

For this experiment, the DeepSole System was expanded to have additional features. The original system had only two modules, one in each shoe, but in this experiment six boards were used. Two mounted at the shoes, two mounted at each thigh, and two mounted at each shank. The thigh boards controlled two vibration motors each, mounted at the rectus femoris and biceps femoris of the corresponding side. The shank boards controlled one vibrator each mounted at the tibial anterior. The leg boards were secured to the subjects using a 3d printed case and Velcro straps, and the vibrators were positioned along the direction of the muscle and secured using medical tape.

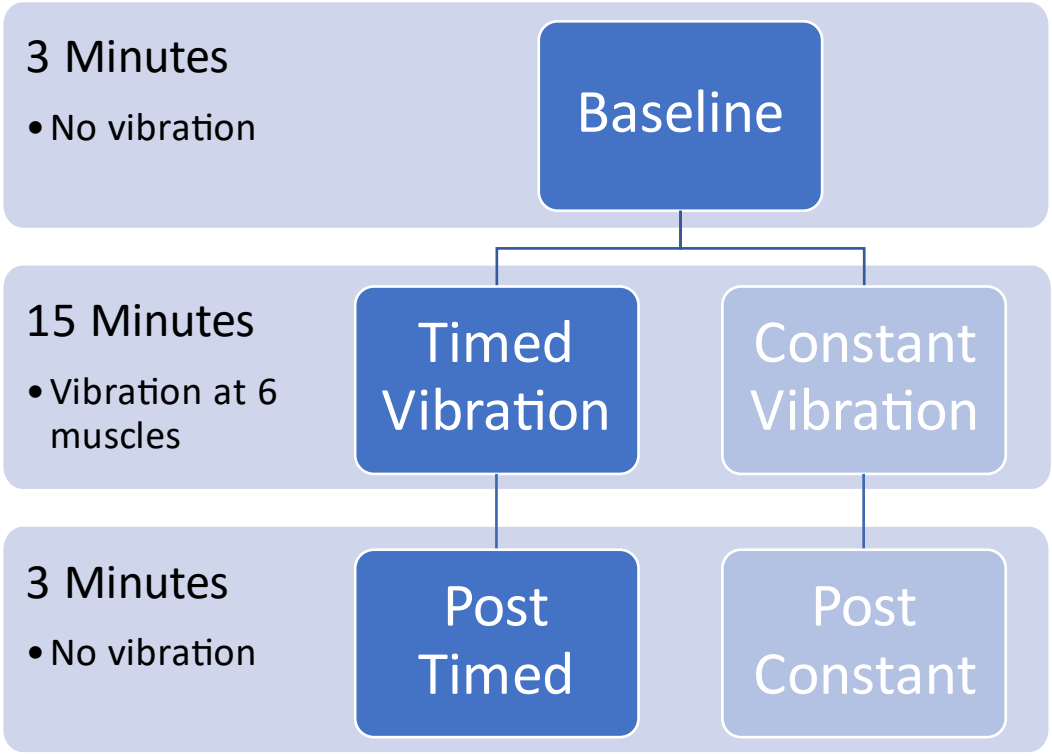

Figure 6.1 Overview of the gait percentage timed vibration protocol. The experiment had 5 sessions where the subjects walked back and forth on the Zeno Walkway while wearing the DeepSole system

For the baseline (BA), post constant (PC), and post timed (PT) sessions, the subjects walked at a self-selected speed for 3 minutes. For these sessions, the DeepSole system was used only for data collection and no feedback was given to the subject. The order of the constant vibration (CV), and timed vibration (TV) was counterbalanced. Four subjects experienced TV first and three subjects experience CV first.

The CV session consisted of 15 minutes of waking. During this time, the DeepSole system streamed the sensor data to a computer. All six vibrators were turned on at a frequency of 80 Hz for the duration of the session. The subjects were asked to walk back and forth on the instrumented mat at a self-selected speed.

For the TV session, bilateral haptic stimulation was provided based on the current gait cycle percentage. The subjects walked for several minutes wearing the DeepSole system enhanced with 6 vibrator motors placed at the right and left side: tibial anterior, rectus femoris, and biceps femoris. Subjects walked for 15 minutes and the data was streamed to a computer where the gait cycle percentage was calculated. The muscle groups used during the experiment are shown in Figure 6.2.

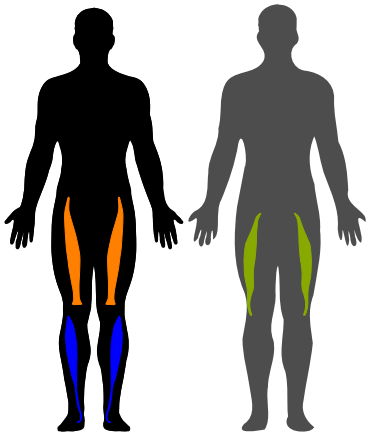

Figure 6.2 Muscles targeted by the synchronized vibration. Left is a frontal view of a person, and left is the back view. Tibial anterior is shown in blue. Rectus femoris is shown

The vibration feedback activation was a function of the gait cycle measured from the right leg of the subject. From 0-10% the right tibial anterior was activated; 10 – 30 % the right rectus femoris; from 30-40 % the left biceps femoris; 40 – 60 % the left tibial anterior; 60 – 75 % rectus femoris; and from 87 – 100 % right biceps femoris. This pattern was repeated during the full training session. The protocol is graphically shown in Table 10.

Table 10 Gait cycle percentage synchronized haptic feedback on muscle groups

Muscles		0 – 10 %	10 – 30 %	30 – 40 %	40 – 60 %	60 – 75 %	87 – 100 %
Right leg	Tibial Anterior						
	Rectus Femoris						
	Biceps Femoris						
Left Leg	Tibial Anterior						
	Rectus Femoris						
	Biceps Femoris						

6.1.1 Gait Cycle Prediction Accuracy

To verify the performance of the neural network model, the real-time prediction was recorded during the TV session. This recording was tested against the recording from the Zeno Walkway. For each prediction made by the model, the corresponding data point in the Zeno recording was found and the error was calculated.

Two metrics were chosen to evaluate the model. The first one was the mean error; this metric should be centered around zero to assure that the predicted gait cycle is running synchronized with actual gait. The second metric chosen was the Root Mean Square Error

(RMSE); this metric was chosen to show the spread of the prediction with respect to the ground truth.

6.1.2 Gait Parameters

To see the effects of the vibration feedback on the gait of the subjects, eight gait parameters were chosen. Stride length (SL), stride width (SW), and step length (TL) were chosen to see the effects on the spatial characteristic of the gait [74]. For the temporal characteristics, stance time (ST), swing time (WT), and stride time (TT) were chosen. A graphical representation of these parameters is shown in Figure 6.3.

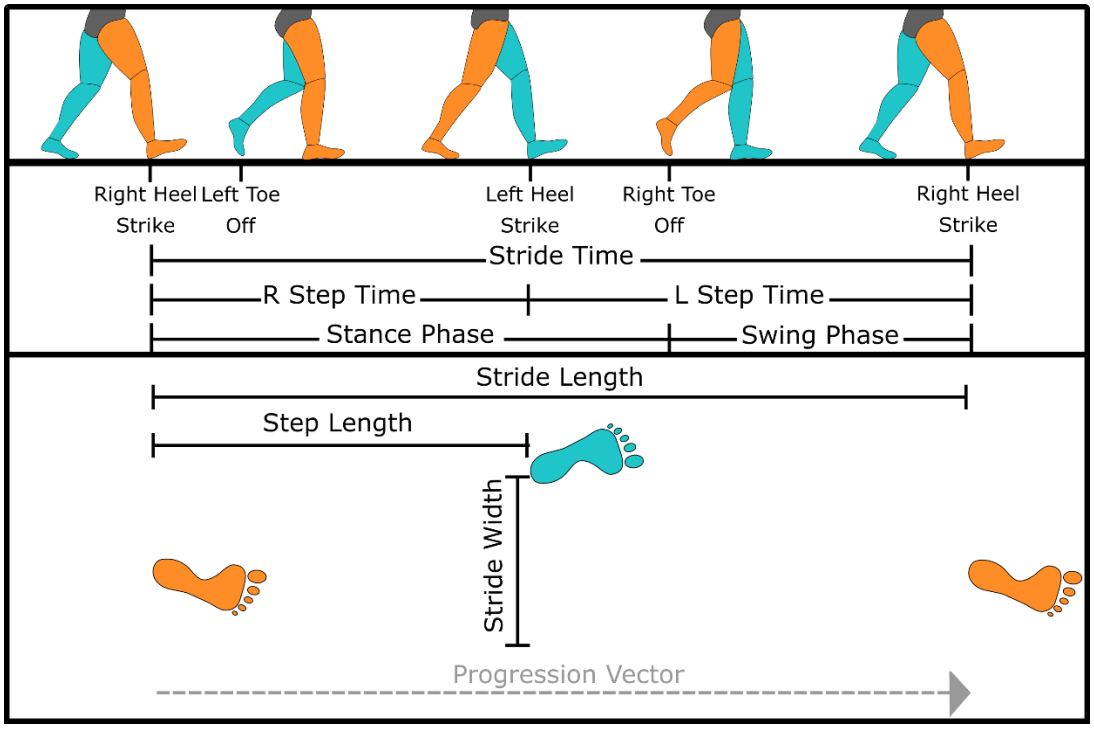

Figure 6.3 Top: Graphical representation of the gait events in a typical gait cycle. These events are used to calculate the temporal and spatial parameters of the gait. The horizontal like shows the start and end of the temporal parameters of the gait: stance time, swing time, stride time, step time. Bottom: Graphical representation on how stride length, stride width, and step length are measured. Blue footprints are from the left side and orange are from the right. The gray arrow is the walking direction. The black lines are the different measurements.

ST is the duration that the corresponding foot is in contact with the ground, this is between heel strike and toe off. WT is the duration between toe off to the subsequent heel strike of the same side, i.e., the period that the foot is not in contact with the floor. TT is the duration between heel strike to heel strike of the same side, this also corresponds to ST + WT.

The progression vector is defined from the location of the heel strike from one side to the subsequent heel strike of the same side. The norm of this vector is the SL. SW is defined as the perpendicular distance from the progression vector to the heel strike of the opposite side. TL is defined as the distance from the location of the heel strike to the heel strike of the opposite side, measured along the progression vector.

Along with the temporal and spatial parameters, two velocity parameters were used. Stride velocity (SV) is the average velocity of one side, this is SL divided by TT. Cadence (CE) is the average number of steps per minute. A step is the period from heel strike from one side the next heel strike of the other side.

6.1.3 Statistical Analysis

For each parameter, two analyses were made. The first was to compare the changes in the sessions BA, CV, and PC to understand the effects of constant vibration on gait. To understand the effects of the gait cycle percentage timed vibration on the gait of the subjects, BA, TC, and PT sessions were compared.

Data for SL, SW, TL, and SV were normally distributed, as indicated by the Kolgomorov-Smirnov test and Q-Q plots. Thus, 1-way repeated measurement ANOVA (rmANOVA) statistical analyses were used. The rmANOVA test was used to evaluate significant differences among the sessions for each of the corresponding vibration type. In the case of significance, pairwise

comparison tests were carried out as post-hoc testing using Bonferroni correction for the number of comparisons. Statistical significance was defined for *: $p < 0.05$.

Data for ST, WT, TT, and CE were not normally distributed, as indicated by the Kolgomorov-Smirnov test and Q-Q plots. Thus, non-parametric statistical analyses were used. The Friedman test was used to evaluate significant differences among the sessions for each of the corresponding vibration type. In the case of significance, Wilcoxon signed-rank tests were carried out as post-hoc testing using Bonferroni correction for the number of comparisons. Statistical significance was defined for *: $p < 0.05$, **: $p < 0.01$, and tests were run using IBM SPSS Statistics 26.

6.2 Results

The accuracy of the model was aggregated and averaged among all subjects. The model had an accuracy of 0.83 ± 1.02 % of the gait cycle and an RMSE of 15.02 ± 1.82 % with respect to the Zeno walkway.

The summary of all gait parameters measured are shown in

. The columns of the table are the different walking sessions, and the rows are the gait parameters.

Table 11 Gait Parameters Summary

		Baseline	**Constant Vibration**	**Post Constant**	**Timed Vibration**	**Post Timed**
Stride Length	Mean ± std	137.6 ± 11.8	139.3 ± 13.2	140.4 ± 13.1	138.4 ± 12.9	140.0 ± 12.6
	Median ± IQR	135.1 ± 10.9	136.6 ± 12.4	137.7 ± 12.2	136.1 ± 12.5	137.3 ± 11.6

Stride Width	Mean ± std	10.47 ± 4.61	9.88 ± 4.52	9.83 ± 4.31	10.08 ± 4.65	9.92 ± 4.76
	Median ± IQR	11.18 ± 6.73	10.57 ± 5.51	10.39 ± 5.34	10.47 ± 5.17	9.85 ± 5.86
Step Length	Mean ± std	68.8 ± 5.9	69.7 ± 6.6	70.3 ± 6.5	69.3 ± 6.5	70.1 ± 6.3
	Median ± IQR	67.6 ± 5.6	68.3 ± 6.2	69.0 ± 6.1	68.1 ± 6.4	68.8 ± 5.9
Stance Time	Mean ± std	0.74 ± 0.07	0.75 ± 0.06	0.73 ± 0.06	0.76 ± 0.06	0.74 ± 0.06
	Median ± IQR	0.76 ± 0.03	0.78 ± 0.04	0.75 ± 0.04	0.77 ± 0.05	0.76 ± 0.05
Swing Time	Mean ± std	0.40 ± 0.02	0.41 ± 0.02	0.40 ± 0.02	0.41 ± 0.02	0.40 ± 0.02
	Median ± IQR	0.41 ± 0.01	0.41 ± 0.02	0.40 ± 0.02	0.41 ± 0.02	0.40 ± 0.02
Stride Time	Mean ± std	1.14 ± 0.09	1.15 ± 0.07	1.13 ± 0.08	1.16 ± 0.08	1.14 ± 0.07
	Median ± IQR	1.17 ± 0.03	1.18 ± 0.05	1.16 ± 0.04	1.17 ± 0.05	1.16 ± 0.05
Stride Velocity	Mean ± std	122.81 ± 20.73	122.58 ± 19.78	125.64 ± 20.38	120.76 ± 19.50	124.16 ± 18.66
	Median ± IQR	112.72 ± 12.45	110.75 ± 14.75	114.90 ± 11.11	112.67 ± 12.95	116.33 ± 14.12
Cadence	Mean ± std	106.63 ± 9.94	105.07 ± 7.48	106.89 ± 8.13	104.18 ± 7.62	106.05 ± 7.40
	Median ± IQR	102.90 ± 2.64	101.44 ± 4.02	103.99 ± 3.88	102.35 ± 4.33	103.90 ± 4.88

6.2.1 Constant Vibration

The subjects changed their gait during the BA, CV, and PC sessions. All the gait parameters for each subject were averaged per session and then grouped within subjects.

For the constant vibration analyses, main effects were found in the spatial parameters: SL ($F(2) = 7.08$, $p = 0.023$), TL ($F(2) = 7.959$, $p = 0.006$). Also, main effects were found in the velocity parameters SV ($F(2) = 6.778$, $p = 0.011$), and CE ($x(2) = 6.0$, $p = 0.049$).

Given that main effects were found, post-hoc pairwise comparison were carried out. For SL, BA and PC sessions were statistically different (p = 0.023). For TL, statistically differences were found between the BA and PC (p = 0.015) sessions. For SV, BA was different from PC (p = 0.041), and CV from PC (p = 0.046). Lastly, for CE, CV and PC were statistically different (z = 2.673, p = 0.023). Results are shown in Figure 6.4.

For SW (F (2), p = 0.174), ST (x (2) = 2.571, p = 0.276), TT (x (2) = 3.714, p = 0.156), and WT (x (2) = 2.0, p = 0.368) no statistical difference was found.

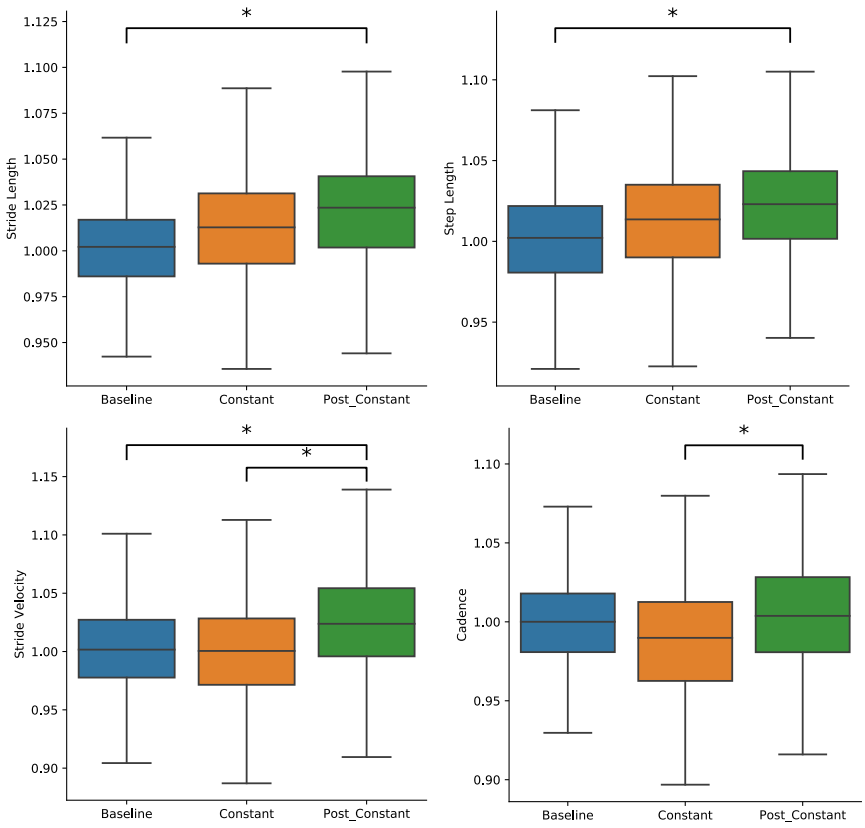

Figure 6.4 Box plot of the gait parameters for constant vibration. For all plots, the horizontal axis shows the session, and the vertical axis is the value in the corresponding units. The horizontal lines with the * symbol above the boxes represent statistical significant between the sessions. Top left plot

is stride length in centimeters, top right is step length in centimeters. Bottom left is stride velocity in centimeter per second, and the bottom right is cadence in steps per minute.

The subjects changed their gait during the BA, TV, and PT sessions. All the gait parameters for each subject were averaged per session and then grouped within subjects.

6.2.2 Timed Vibration

For the timed vibration analyses, main effects were found in the temporal gait parameters ST ($x(2) = 8.0$, $p = 0.018$), TT ($x(2) = 8.0$, $p = 0.018$). As well as in the velocity parameters SV ($F(2) = 6.310$, $p = 0.043$), and CE ($x(2) = 8.0$, $p = 0.018$).

Post-hoc pairwise comparison showed that for ST, BA was different from TV ($z = -2.673$, p 0.023). For TT, the TV session was different from PT ($z = 2.673$, $p = 0.023$). As for SV, TV and PT were sessions different ($p = 0.024$). For CE, TV and PT were also statistically different ($z = 2.673$, p0.023). Results are shown in Figure 6.5.

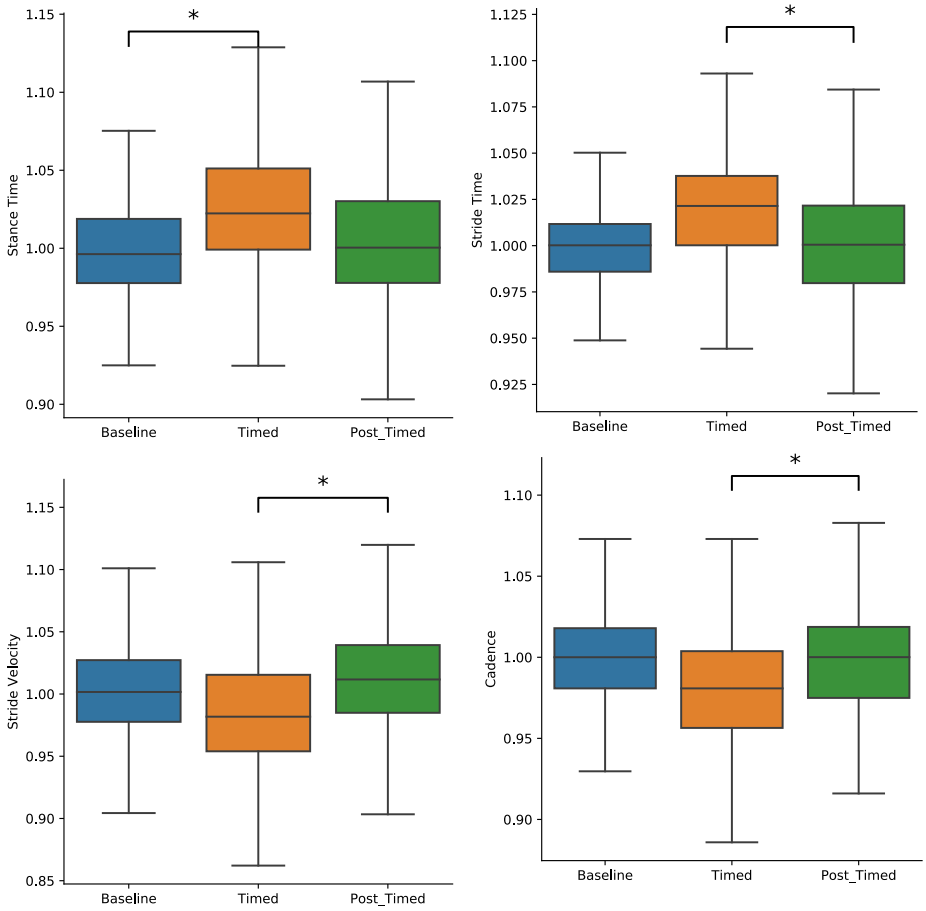

Figure 6.5 Box plot of the gait parameters for gait cycle percentage timed vibration. For all plots, the horizontal axis shows the session, and the vertical axis is the value in the corresponding units. The horizontal lines with the * symbol above the boxes represent statistical significant between the sessions. Top left plot is stance time in seconds, and the top right is stride time in seconds. Bottom left is stride velocity in centimeter per second, and the bottom right is cadence in steps per minute.

6.3 Discussion

The offline model was able to achieve an RMSE of 7.2 ± 2.4 %, this is considerably better than the performance online of 15.02 ± 1.82 %. This could be because when running online, a few data packages are lost through the network communication. Furthermore, the subjects' gait is altered during the TV session. Although, the performance is worse online than offline, the error is still centered around zero. This means that the gait is closely tracked by the model. Furthermore, RMSE does not consider that during the end of the cycle and the start of the new one, there is a

sudden jump in the value. Therefore, the error between 99% of the previous cycle and 1% of the current cycle is 2%, not 98%. This could make the RMSE artificially higher than the actual value.

The results show that the subjects modified their gait when a vibration was applied to their muscles. As for the two types of vibratory feedback, our hypothesis that the subjects would modify their cadence and stride velocity was confirmed to be true. Both strategies found statistical differences in these two parameters. This is congruent with the previous literature, although the feedback affects the gait of the subjects differently. For the constant vibration, the SV was different between PC and all other sessions, and the cadence was difference only during the CV and PC sessions. As for the timed vibration, both the velocity and cadence were only different during TV and PC.

The constant vibration has a higher effect on the temporal parameters of the gait, making both the stride and step length statistically different while no difference was found between the temporal parameters. On the other hand, the timed vibration had a greater effect on the temporal parameters of the gait. Making the stance and stride times statistically different, but not the stride and step length. By only affecting either the spatial or temporal parameters, both feedbacks influence the velocity parameters.

As shown by Proske et al [100] the signal from the spindles changes depending on the current state of the muscle and its history of activation. Therefore, the vibration feedback affects the muscle spindle differently depending on whether the muscle is being contracted or not. The timed vibration is designed to be active at the same time the muscle is active, the end result of this effect is that the vibration has a higher effect on the spatial parameters. By only providing the vibration when the muscle is being contracted, the information about the length of the muscle is affected.

Furthermore, during the constant vibration sessions, vibration is provided at all muscles at once. This means that the agonist and antagonist muscles are being excited by the feedback at the same time. As shown by Ribot-Ciscar et al [105] when a vibration is applied to muscles pair the central nervous system uses the difference of the information from the muscle spindles for positional information. Given this property, the positional information is not affected by the vibration, therefore not statistically different was found on the spatial parameters.

The results show that the effects of the vibration carry over even when the vibration is not present anymore. This is shown by the statistical analysis, as PC and PT are the sessions were most of the gait parameters are different. This could be because the signal of the spindles changes depending on the history of activation. Therefore, the effects of the vibration during the training sessions carry over to the post sessions.

6.4 Conclusion

The conducted experiment shows that the gait cycle prediction model can be used to provide feedback to subjects while walking. This model, paired with the DeepSole, is capable of timely tracking the gait of the subjects, even if its' performance online is worse than offline.

With the two types of haptic feedback, the subjects modified their gait. With both feedbacks, their stride velocity and cadence were modified. But this is because these parameters depend on both spatial and temporal parameters. Constant vibration modified the spatial parameters, while timed vibration modified the temporal parameters. The results shows that the strategy of when and where the vibration is applied can have an impact on the gait of people. This can be explored further to create procedures that target specific parameters of the gait. This could be used for rehabilitation on different populations with gait impairments.

This experiment was conducted on healthy young adults and both types of vibration had a significant effect on their gait. It would be interesting to conduct a similar experiment with a broader population to investigate the effects on gait and other variables, like balance. For example, one could investigate if exciting the muscle spindles has a significant impact on elder people with balance problems.

Chapter 7: Conclusions

The DeepSole system combined with the different neural network models is a fully capable to characterize the gait of the individuals and provide vibratory feedback to the wearer. Thanks to the flexible construction and its wireless capabilities, it can be comfortably worn by wide arrange of people, both normally developed and people with pathologies that affect their gait.

The system can transmit the data wirelessly and can process the gait in real time at a high frequency of 50Hz. This was tested with experiments on both the gait phase and continuously tracking the gait cycle percentage. Using these two strategies, subjects were able to modify their gait. Thanks to these characteristics, the system can be paired with any device to provide different types of feedbacks. During the studies presented in this dissertation, the system was used with over 100 subjects of different ages, sizes, and pathologies. The system is shown to be reliable and durable.

7.1 Novelty in DeepSole System Design

The Deepsole system utilizes a modular design that is integrated into a single system that works together to characterize the gait of a person. By using state-of-the-art e-textiles, the insole module is comfortable and can provide an accurate reading of the loading at the foot level. The e-textile insole can be made to a wide range of sizes to accommodate different ages and anthropometrics. Furthermore, the sensorized area could be adapted to every size. All components are contained within the shoe, no wires are run through the wearer, and all communications are done wirelessly.

The system can record a total of 24 sensors simultaneously at a sampling rate of up to 200 Hz, this property allows it to record different activities other than walking [113], [114]. Although, the system has many sensors, the power consumption is low. We estimate that using an 850 mAh battery with a sampling frequency of 50Hz, the system can do continues data recording for up to 6 hours. These properties open the possibility to use the system for longitudinal studies. The DeepSole system could be used to record patients during daily life activities to understand the effect of different pathologies, like Parkinson Disease where some gait phenomena are hard to replicate in clinical settings [115].

The electronics module is autonomous, can record 9 kinematics sensors and can independently control up to 3 direct current motors. Thanks to the wireless capabilities of the system, it can be upgraded to record motion data not only at the feet level but at other body segments. This property was used in the study presented in Chapter 6 to provide gait cycle timed vibration. Moreover, these modules could be expanded to make the DeepSole system a full-body motion tracker.

7.2 Neural Networks for Gait Analysis and Training

The design novelties of the DeepSole system allowed to do long recording sessions on a vast number of subjects. This created the need to process all these data in a fast an accurate fashion. To achieve this, artificial neural networks was chosen. ANNs was chosen because of their flexibility on mapping two different workspaces. Using the gait recordings, we were able to map the sensor reading to different gait spatiotemporal parameters. The models created are capable of processing minutes of recordings in a few seconds and have a comparable performance on various subjects, even when the subjects were not involved on the training.

Three models are presented in this dissertation. The first one is a recurrent neural network that can classify the recording into the corresponding gait phase, i.e., stance phase or swing phase. Once the recording is divided into the corresponding phase, this output can be used to identify specific gait events like heel strike and toe off. Then, the heel strike can be used to divide the recording into strides. Once the data is segmented into stride, integration methods can be used to derive the several spatial parameters from the IMU recordings [116], [117]. Additionally, this model can be used in real-time to provide haptic feedback at specific gait phases, like shown in Chapter 5. In that study, vibratory feedback was provided to elicit an increased stance time on the non-dominant side of typically developed adults. This strategy resulted in asymmetrical walking, but only on the temporal parameters and not on the spatial parameters. The asymmetry in the temporal parameters implies that the subjects were loading their non-dominant leg for a longer time. These results could be used with population with muscle deficits on one side of the body, like stroke survivors.

The second model presented uses an encoder-decoder recurrent neural network to provide a continuous prediction of the gait cycle percentage. This model excels at closely tracking the gait, even if the gait frequency suddenly changes (for example from a force being applied to the subject). This is thanks to the neural network architecture implemented that allows the raw sensor data to be processed without any filtering or preprocessing. Also, the dataset included data from a varied group of individuals with different anthropometrics and cadences. Furthermore, the left and right sides are treated as independent, this gives the model the ability to track the gait of subjects who present asymmetric walking. In Chapter 6, we used this model to provide complex vibratory feedback to healthy individuals. The feedback comprised of vibrations at the muscle level, the activation of feedback was a function of the gait cycle. The function was related the moment when

the muscle is active. To understand the effect of the timed vibration, constant vibration at the muscle level was also applied. The results showed that the kinematics of the subjects are affected by the vibration. But timed and constant vibration affect the gait different. The constant vibration has a higher effect on the temporal parameters and the timed vibration has a higher effect on the spatial parameters. The reason of the different effects needs to be further investigated. The differences can come from where the vibration is being processed. For example, the difference can come from one type of vibration being process by the central neural system and the other type being processed by the muscles spindles.

The close tracking of the gait cycle of the DeepSole system can be used to provide gait synchronized feedback. The technology can have a big impact in different populations. For instance, in children with CP, it is often observed that they move their trunk and pelvis excessively as compared to normal gait [118]. Several of these characteristic movements have been studied, such as Trendelenburg gait. In Trendelenburg gait, the person is seen dropping their hip during the unloaded part of their gait [118]. Thus, Trendelenburg gait may also be referred to as hip drop. This is thought to be caused by weakness of certain muscle groups in the lower limb, including the gluteus medius and gluteus minimus [119]. For this study, a frontal moment could be applied to the pelvis. This frontal plane pelvic moment would be coordinated with the user's gait, as shown in **Error! Reference source not found.**. The hypothesis is that by applying the moments timed to the gait, the muscles used during gait would be stimulated, thus strengthening them.

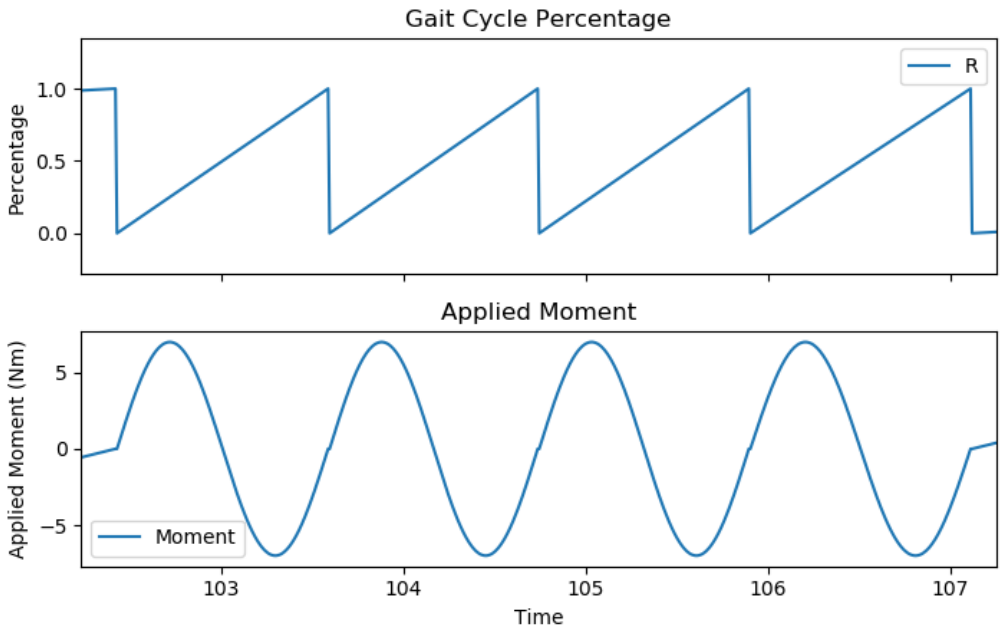

Figure 7.1 Example of the applied moment to the pelvis synchronized to the gait of the subject. Top shows the gait cycle percentage as time passes. Bottom shows a sinusoidal function of the pelvis moment.

The third model presented uses 2D encoder-decoder recurrent neural network to identify when a patient with Parkinson's Disease is in a freezing of gait episode. During this episode, the patients' voluntary walking stops, and they cannot continue walking. The episode can last from a fraction of a second, up to several seconds. This episode is difficult to replicate in clinical setting, thus studying it is challenging [115]. Automatically identifying the freezing of gait events is challenging because the algorithm needs to differentiate between voluntary and involuntary stopping. For the presented model, we wanted to use the experience of clinical experts to create a machine learning model that can identify the involuntary stopping of gait. To achieve this, we paired the recording from the DeepSole sensors with a coded video of the walking session. The video codding was done by a clinical expert and the information from both left and right shoes were used. The goal of the model was to classify the walking data into regular gait and freezing of

gait at a high frequency (50 Hz). The high frequency identification could be used to provide feedback when the patient is in a freezing event.

Furthermore, the recording could be used to study an understand the onset of the event. To achieve this, several patients with Parkinson's Disease who present FOG could wear the DeepSole system while performing their daily life activities. The model could be used to classify the recording to understand the triggers of the event.

The work presented show the versatility of the DeepSole system when paired with neural networks. It can be used for characterization, training, and can act as an abstract sensor for human gait. The system can be used to do long recordings of people with gait abnormalities outside of a clinical setting. This could help understand how the disease affects their day-to-day living. Furthermore, the techniques presented for multi-sensor mapping can be easily adapted to multiple devices and sensors. These techniques can be expanded to identify episodic events in pathologies, and retrain gait irregularities, like asymmetry and muscle weakness.

References

[1] S. R. Simon, “Quantification of human motion: gait analysis—benefits and limitations to its application to clinical problems,” *J. Biomech.*, vol. 37, no. 12, pp. 1869–1880, Dec. 2004.

[2] R. M. Kay, S. Dennis, S. Rethlefsen, R. A. Reynolds, D. L. Skaggs, and V. T. Tolo, “The effect of preoperative gait analysis on orthopaedic decision making.,” *Clin. Orthop. Relat. Res.*, no. 372, pp. 217–22, Mar. 2000.

[3] T. A. L. Wren *et al.*, “Effects of Preoperative Gait Analysis on Costs and Amount of Surgery,” *J. Pediatr. Orthop.*, vol. 29, no. 6, pp. 558–563, Sep. 2009.

[4] B. J. Darter and J. M. Wilken, “Gait training with virtual reality--based real-time feedback: improving gait performance following transfemoral amputation,” *Phys. Ther.*, vol. 91, no. 9, pp. 1385–1394, 2011.

[5] M. Roerdink, C. J. C. Lamoth, P. J. Beek, and others, “Online gait event detection using a large force platform embedded in a treadmill,” *J. Biomech.*, vol. 41, no. 12, pp. 2628–2632, 2008.

[6] W. Xu, M.-C. Huang, N. Amini, J. J. Liu, L. He, and M. Sarrafzadeh, “Smart insole: A Wearable System for Gait Analysis,” in *Proceedings of the 5th International Conference on PErvasive Technologies Related to Assistive Environments - PETRA ’12*, 2012, p. 1.

[7] K. N. Winfree, I. Pretzer-Aboff, D. Hilgart, R. Aggarwal, M. Behari, and S. K. Agrawal, “The effect of step-synchronized vibration on patients with parkinson’s disease: Case studies on subjects with freezing of gait or an implanted deep brain stimulator,” *IEEE Trans. Neural Syst. Rehabil. Eng.*, vol. 21, no. 5, pp. 806–811, Sep. 2013.

[8] Jeffrey M.Hausdorff, “Gait dynamics, fractals and falls: Finding meaning in the stride-to-stride fluctuations of human walking,” *Hum. Mov. Sci.*, vol. 26, no. 4, pp. 555–589, Aug. 2007.

[9] B. E. Maki, “Gait Changes in Older Adults: Predictors of Falls or Indicators of Fear?,” *J. Am. Geriatr. Soc.*, vol. 45, no. 3, pp. 313–320, Mar. 1997.

[10] J. Verghese, R. B. Lipton, C. B. Hall, G. Kuslansky, M. J. Katz, and H. Buschke, “Abnormality of Gait as a Predictor of Non-Alzheimer’s Dementia,” *N. Engl. J. Med.*, vol. 347, no. 22, pp. 1761–1768, Nov. 2002.

[11] T. Buracchio, H. H. Dodge, D. Howieson, D. Wasserman, and J. Kaye, “The Trajectory of Gait Speed Preceding Mild Cognitive Impairment,” *Arch. Neurol.*, vol. 67, no. 8, pp. 980–986, Aug. 2010.

[12] A. Prado, X. Cao, M. T. Robert, A. M. Gordon, and S. K. Agrawal, "Gait Segmentation of Data Collected by Instrumented Shoes Using a Recurrent Neural Network Classifier," *Phys. Med. Rehabil. Clin. N. Am.*, vol. 30, no. 2, 2019.

[13] S. Patel, H. Park, P. Bonato, L. Chan, and M. Rodgers, "A review of wearable sensors and systems with application in rehabilitation," *J. Neuroeng. Rehabil.*, vol. 9, no. 1, p. 21, 2012.

[14] M. Stoppa and A. Chiolerio, "Wearable electronics and smart textiles: a critical review," *sensors*, vol. 14, no. 7, pp. 11957–11992, 2014.

[15] J. A. BUNN, J. W. Navalta, C. J. Fountaine, and J. D. REECE, "Current state of commercial wearable technology in physical activity monitoring 2015--2017," *Int. J. Exerc. Sci.*, vol. 11, no. 7, p. 503, 2018.

[16] D. A. Winter, *Biomechanics and motor control of human movement*. Wiley, 2009.

[17] J. M. Hausdorff, Z. Ladin, and J. Y. Wei, "Footswitch system for measurement of the temporal parameters of gait.," *J. Biomech.*, vol. 28, no. 3, pp. 347–51, Mar. 1995.

[18] H. F. Maqbool *et al.*, "Real-time gait event detection for lower limb amputees using a single wearable sensor," in *2016 38th Annual International Conference of the IEEE Engineering in Medicine and Biology Society (EMBC)*, 2016, pp. 5067–5070.

[19] A. Mannini, V. Genovese, and A. M. Sabatini, "Online decoding of hidden Markov models for gait event detection using foot-mounted gyroscopes," *IEEE J. Biomed. Heal. informatics*, vol. 18, no. 4, pp. 1122–1130, 2013.

[20] Y. C. Han, K. I. Wong, and I. Murray, "Gait Phase Detection for Normal and Abnormal Gaits Using IMU," *IEEE Sens. J.*, vol. 19, no. 9, pp. 3439–3448, May 2019.

[21] I. Karuei, O. S. Schneider, B. Stern, M. Chuang, and K. E. MacLean, "RRACE: Robust realtime algorithm for cadence estimation," *Pervasive Mob. Comput.*, vol. 13, pp. 52–66, 2014.

[22] R. Delgado-Gonzalo *et al.*, "Real-time gait analysis with accelerometer-based smart shoes," in *2017 39th Annual International Conference of the IEEE Engineering in Medicine and Biology Society (EMBC)*, 2017, pp. 148-148c.

[23] J. Hannink *et al.*, "Sensor-based Gait Parameter Extraction with Deep Convolutional Neural Networks," *IEEE J. Biomed. Heal. Informatics*, vol. 2194, no. c, pp. 1–8, Jan. 2016.

[24] A. Mannini and A. M. Sabatini, "A hidden Markov model-based technique for gait segmentation using a foot-mounted gyroscope," in *2011 Annual International Conference of the IEEE Engineering in Medicine and Biology Society*, 2011, pp. 4369–4373.

[25] I. H. López-Nava, A. Muñoz-Meléndez, A. I. Pérez Sanpablo, A. Alessi Montero, I. Quiñones Urióstegui, and L. Núñez Carrera, "Estimation of temporal gait parameters using Bayesian models on acceleration signals," *Comput. Methods Biomech. Biomed. Engin.*, vol. 19, no. 4, pp. 396–403, Mar. 2016.

[26] A. Graves, *Supervised sequence labelling with recurrent neural networks*. Springer, 2012.

[27] I. Goodfellow, Y. Bengio, and A. Courville, *Deep Learning*. MIT Press, 2016.

[28] J. B. Yang, M. N. Nguyen, P. P. San, X. L. Li, and K. Shonali, "Deep Convolutional Neural Networks On Multichannel Time Series For Human Activity Recognition," *IJCAI'15 Proc. 24th Int. Conf. Artif. Intell.*, 2015.

[29] I. Sutskever, O. Vinyals, and Q. V. Le, "Sequence to Sequence Learning with Neural Networks," Sep. 2014.

[30] Z. C. Lipton, J. Berkowitz, and C. Elkan, "A Critical Review of Recurrent Neural Networks for Sequence Learning," May 2015.

[31] ATS Committee on Proficiency Standards for Clinical Pulmonary Function Laboratories, "ATS Statement," *Am. J. Respir. Crit. Care Med.*, vol. 166, no. 1, pp. 111–117, Jul. 2002.

[32] K. Cho *et al.*, "Learning Phrase Representations using RNN Encoder-Decoder for Statistical Machine Translation," Jun. 2014.

[33] M. Hüsken and P. Stagge, "Recurrent neural networks for time series classification," *Neurocomputing*, vol. 50, pp. 223–235, Jan. 2003.

[34] D. P. Kingma and J. Ba, "Adam: A Method for Stochastic Optimization," Dec. 2014.

[35] R. O. Duda, P. E. (Peter E. Hart, and D. G. Stork, *Pattern classification*. John Wiley & Sons, 2012.

[36] J. M. Bland and D. G. Altman, "Statistical methods for assessing agreement between two methods of clinical measurement.," *Lancet (London, England)*, vol. 1, no. 8476, pp. 307–10, Feb. 1986.

[37] T. A. L. Wren, S. Rethlefsen, and R. M. Kay, "Prevalence of specific gait abnormalities in children with cerebral palsy: Influence of cerebral palsy subtype, age, and previous surgery," *Journal of Pediatric Orthopaedics*. 2005.

[38] A. Kharb, V. Saini, Y. K. Jain, and S. Dhiman, "A review of gait cycle and its parameters," *IJCEM Int. J. Comput. Eng. Manag.*, vol. 13, pp. 78–83, 2011.

[39] T. Lenzi, M. C. Carrozza, and S. K. Agrawal, “Powered hip exoskeletons can reduce the user’s hip and ankle muscle activations during walking,” *IEEE Trans. Neural Syst. Rehabil. Eng.*, vol. 21, no. 6, pp. 938–948, 2013.

[40] K. Seo, S. Hyung, B. K. Choi, Y. Lee, and Y. Shim, “A new adaptive frequency oscillator for gait assistance,” in *2015 IEEE International Conference on Robotics and Automation (ICRA)*, 2015, pp. 5565–5571.

[41] D. Zanotto, P. Stegall, and S. K. Agrawal, “Adaptive assist-as-needed controller to improve gait symmetry in robot-assisted gait training,” in *2014 IEEE international conference on robotics and automation (ICRA)*, 2014, pp. 724–729.

[42] R. Ronsse, N. Vitiello, T. Lenzi, J. Van Den Kieboom, M. C. Carrozza, and A. J. Ijspeert, “Human--robot synchrony: flexible assistance using adaptive oscillators,” *IEEE Trans. Biomed. Eng.*, vol. 58, no. 4, pp. 1001–1012, 2010.

[43] W. van Dijk, H. van der Kooij, B. Koopman, and E. H. F. van Asseldonk, “Improving the transparency of a rehabilitation robot by exploiting the cyclic behaviour of walking,” in *2013 IEEE 13th International Conference on Rehabilitation Robotics (ICORR)*, 2013, pp. 1–8.

[44] Y. LeCun, L. Bottou, G. Orr, and K. Muller, “Efficient backprop in neural networks: Tricks of the trade,” *Lect. Notes Comput. Sci.*, vol. 1524, no. 98, p. 111, 1998.

[45] W. Pirker and R. Katzenschlager, “Gait disorders in adults and the elderly,” *Wien. Klin. Wochenschr.*, vol. 129, no. 3–4, pp. 81–95, 2017.

[46] H. Vu, F. Gomez, P. Cherelle, D. Lefeber, A. Nowé, and B. Vanderborght, “ED-FNN: A new deep learning algorithm to detect percentage of the gait cycle for powered prostheses,” *Sensors*, vol. 18, no. 7, p. 2389, 2018.

[47] R. H. R. Hahnloser, R. Sarpeshkar, M. A. Mahowald, R. J. Douglas, and H. S. Seung, “Digital selection and analogue amplification coexist in a cortex-inspired silicon circuit,” *Nature*, vol. 405, no. 6789, p. 947, 2000.

[48] J. Chung, C. Gulcehre, K. Cho, and Y. Bengio, “Empirical evaluation of gated recurrent neural networks on sequence modeling,” *arXiv Prepr. arXiv1412.3555*, Dec. 2014.

[49] K. Fragkiadaki, S. Levine, P. Felsen, and J. Malik, “Recurrent network models for human dynamics,” in *Proceedings of the IEEE International Conference on Computer Vision*, 2015, pp. 4346–4354.

[50] N. Srivastava, G. Hinton, A. Krizhevsky, I. Sutskever, and R. Salakhutdinov, “Dropout: A Simple Way to Prevent Neural Networks from Overfitting,” *J. Mach. Learn. Res.*, 2014.

[51] L. M. L. De Lau and M. M. B. Breteler, “Epidemiology of Parkinson’s disease,” *Lancet Neurol.*, vol. 5, no. 6, pp. 525–535, 2006.

[52] B. R. Bloem, J. M. Hausdorff, J. E. Visser, and N. Giladi, “Falls and freezing of gait in Parkinson’s disease: a review of two interconnected, episodic phenomena,” *Mov. Disord. Off. J. Mov. Disord. Soc.*, vol. 19, no. 8, pp. 871–884, 2004.

[53] A. H. Snijders *et al.*, “Physiology of freezing of gait,” *Ann. Neurol.*, vol. 80, no. 5, pp. 644–659, 2016.

[54] N. Giladi *et al.*, “Freezing of gait in patients with advanced Parkinson’s disease,” *J. Neural Transm.*, vol. 108, no. 1, pp. 53–61, 2001.

[55] M. Hallett, “The intrinsic and extrinsic aspects of freezing of gait,” *Mov. Disord.*, vol. 23, no. S2, pp. S439–S443, Jul. 2008.

[56] J. D. Schaafsma, Y. Balash, T. Gurevich, A. L. Bartels, J. M. Hausdorff, and N. Giladi, “Characterization of freezing of gait subtypes and the response of each to levodopa in Parkinson’s disease,” *Eur. J. Neurol.*, vol. 10, no. 4, pp. 391–398, 2003.

[57] A. Fasano and A. M. Lozano, “Deep brain stimulation for movement disorders: 2015 and beyond,” *Curr. Opin. Neurol.*, vol. 28, no. 4, pp. 423–436, 2015.

[58] A. Nieuwboer *et al.*, “Reliability of the new freezing of gait questionnaire: agreement between patients with Parkinson’s disease and their carers,” *Gait Posture*, vol. 30, no. 4, pp. 459–463, 2009.

[59] N. Giladi and A. Nieuwboer, “Understanding and treating freezing of gait in parkinsonism, proposed working definition, and setting the stage,” *Mov. Disord. Off. J. Mov. Disord. Soc.*, vol. 23, no. S2, pp. S423--S425, 2008.

[60] M. Suteerawattananon, G. S. Morris, B. R. Etnyre, J. Jankovic, and E. J. Protas, “Effects of visual and auditory cues on gait in individuals with Parkinson’s disease,” *J. Neurol. Sci.*, vol. 219, no. 1–2, pp. 63–69, 2004.

[61] S. Donovan *et al.*, “Laserlight cues for gait freezing in Parkinson’s disease: an open-label study,” *Parkinsonism Relat. Disord.*, vol. 17, no. 4, pp. 240–245, 2011.

[62] A. Nieuwboer *et al.*, “Cueing training in the home improves gait-related mobility in Parkinson’s disease: the RESCUE trial,” *J. Neurol. Neurosurg. Psychiatry*, vol. 78, no. 2, pp. 134–140, 2007.

[63] A. L. S. De Lima *et al.*, “Freezing of gait and fall detection in Parkinson’s disease using wearable sensors: a systematic review,” *J. Neurol.*, vol. 264, no. 8, pp. 1642–1654, 2017.

[64] C. Ahlrichs *et al.*, “Detecting freezing of gait with a tri-axial accelerometer in Parkinson’s disease patients,” *Med. Biol. Eng. Comput.*, vol. 54, no. 1, pp. 223–233, 2016.

[65] D. Rodríguez-martín *et al.*, “Comparison of Features, Window Sizes and Classifiers in Detecting Freezing of Gait in Patients with Parkinson’s Disease Through a Waist-Worn Accelerometer,” in *Artificial Intelligence Research and Development: Proceedings of the 19th International Conference of the Catalan Association for Artificial Intelligence, Barcelona, Catalonia, Spain, October 19-21, 2016*, 2016, p. 127.

[66] E. E. Tripoliti *et al.*, “Automatic detection of freezing of gait events in patients with Parkinson’s disease,” *Comput. Methods Programs Biomed.*, vol. 110, no. 1, pp. 12–26, 2013.

[67] S. Mazilu, A. Calatroni, E. Gazit, A. Mirelman, J. M. Hausdorff, and G. Tröster, “Prediction of freezing of gait in Parkinson’s from physiological wearables: an exploratory study,” *IEEE J. Biomed. Heal. informatics*, vol. 19, no. 6, pp. 1843–1854, Nov. 2015.

[68] M. Capecci, L. Pepa, F. Verdini, and M. G. Ceravolo, “A smartphone-based architecture to detect and quantify freezing of gait in Parkinson’s disease,” *Gait Posture*, vol. 50, pp. 28–33, 2016.

[69] S. Rezvanian and T. E. Lockhart, “Towards real-time detection of freezing of gait using wavelet transform on wireless accelerometer data,” *Sensors*, vol. 16, no. 4, p. 475, 2016.

[70] A. El-Attar, A. S. Ashour, N. Dey, H. Abdelkader, M. M. Abd El-Naby, and R. S. Sherratt, “Discrete wavelet transform-based freezing of gait detection in Parkinson’s disease,” *J. Exp. Theor. Artif. Intell.*, pp. 1–17, 2018.

[71] A. Marcante *et al.*, “Foot Pressure Wearable Sensors for Freezing of Gait Detection in Parkinson’s Disease,” *Sensors*, vol. 21, no. 1, p. 128, Dec. 2020.

[72] Y. Xia, J. Zhang, Q. Ye, N. Cheng, Y. Lu, and D. Zhang, “Evaluation of deep convolutional neural networks for detection of freezing of gait in Parkinson’s disease patients,” *Biomed. Signal Process. Control*, vol. 46, pp. 221–230, Sep. 2018.

[73] P. Lorenzi *et al.*, “Smart sensors for the recognition of specific human motion disorders in Parkinson’s disease,” in *2015 6th International Workshop on Advances in Sensors and Interfaces (IWASI)*, 2015, pp. 131–136.

[74] F. Huxham, J. Gong, R. Baker, M. Morris, and R. Iansek, “Defining spatial parameters for non-linear walking,” *Gait Posture*, vol. 23, no. 2, pp. 159–163, Feb. 2006.

[75] S. Seabold and J. Perktold, “Statsmodels: Econometric and Statistical Modeling with Python,” 2010.

[76] A. Prado, X. Cao, X. Ding, and S. K. Agrawal, “Prediction of Gait Cycle Percentage Using Instrumented Shoes with Artificial Neural Networks,” in *Proceedings - IEEE International Conference on Robotics and Automation*, 2020.

[77] D. P. Kingma and J. Ba, “Adam: {A} Method for Stochastic Optimization,” *CoRR*, vol. abs/1412.6, 2014.

[78] A. Linden, “Measuring diagnostic and predictive accuracy in disease management: an introduction to receiver operating characteristic (ROC) analysis,” *J. Eval. Clin. Pract.*, vol. 12, no. 2, pp. 132–139, Apr. 2006.

[79] J. V. Tu, “Advantages and disadvantages of using artificial neural networks versus logistic regression for predicting medical outcomes,” *J. Clin. Epidemiol.*, vol. 49, no. 11, pp. 1225–1231, Nov. 1996.

[80] L. Toth, “Combining time- and frequency-domain convolution in convolutional neural network-based phone recognition,” in *ICASSP, IEEE International Conference on Acoustics, Speech and Signal Processing - Proceedings*, 2014, pp. 190–194.

[81] A. Nieuwboer, R. Dom, W. De Weerdt, K. Desloovere, S. Fieuws, and E. Broens-Kaucsik, “Abnormalities of the spatiotemporal characteristics of gait at the onset of freezing in Parkinson’s disease,” *Mov. Disord.*, vol. 16, no. 6, pp. 1066–1075, Nov. 2001.

[82] A. M. De Nunzio, M. Grasso, A. Nardone, M. Godi, and M. Schieppati, “Alternate rhythmic vibratory stimulation of trunk muscles affects walking cadence and velocity in Parkinson’s disease,” *Clin. Neurophysiol.*, 2010.

[83] S. Hwang, P. Agada, S. Grill, T. Kiemel, and J. J. Jeka, “A central processing sensory deficit with Parkinson’s disease,” *Exp. Brain Res.*, 2016.

[84] M. O. Conrad, R. A. Scheidt, and B. D. Schmit, “Effects of wrist tendon vibration on targeted upper-arm movements in poststroke hemiparesis,” *Neurorehabil. Neural Repair*, 2011.

[85] M. H. Thaut, G. C. McIntosh, and R. R. Rice, “Rhythmic facilitation of gait training in hemiparetic stroke rehabilitation,” *J. Neurol. Sci.*, vol. 151, no. 2, pp. 207–212, 1997.

[86] B. J. Fregly, “Gait modification to treat knee osteoarthritis,” *HSS J.*, vol. 8, no. 1, pp. 45–48, 2012.

[87] D. Martelli, L. Luo, J. Kang, U. J. Kang, S. Fahn, and S. K. Agrawal, “Adaptation of stability during perturbed walking in Parkinson’s disease,” *Sci. Rep.*, vol. 7, no. 1, p. 17875, 2017.

[88] X. Jin, A. Prado, and S. K. Agrawal, “Retraining of Human Gait - Are Lightweight Cable-Driven Leg Exoskeleton Designs Effective?,” *IEEE Trans. Neural Syst. Rehabil. Eng.*, vol. 26, no. 4, 2018.

[89] S. Crea, B. B. Edin, K. Knaepen, R. Meeusen, and N. Vitiello, “Time-Discrete Vibrotactile Feedback Contributes to Improved Gait Symmetry in Patients With Lower Limb Amputations: Case Series,” *Phys. Ther.*, vol. 97, no. 2, pp. 198–207, Feb. 2017.

[90] C. Z.-H. Ma, Y.-P. Zheng, and W. C.-C. Lee, “Changes in gait and plantar foot loading upon using vibrotactile wearable biofeedback system in patients with stroke,” *Top. Stroke Rehabil.*, vol. 25, no. 1, pp. 20–27, Jan. 2018.

[91] M. R. Afzal, H. Lee, J. Yoon, M. K. Oh, and C. H. Lee, “Development of an augmented feedback system for training of gait improvement using vibrotactile cues,” in *2017 14th International Conference on Ubiquitous Robots and Ambient Intelligence, URAI 2017*, 2017, pp. 818–823.

[92] M. R. Afzal, H. Lee, A. Eizad, C. H. Lee, M.-K. Oh, and J. Yoon, “Effects of Vibrotactile Biofeedback Coding Schemes on Gait Symmetry Training of Individuals With Stroke,” *IEEE Trans. Neural Syst. Rehabil. Eng.*, vol. 27, no. 8, pp. 1617–1625, Aug. 2019.

[93] K. S. K. S. Hale and K. M. K. M. Stanney, “Deriving haptic design guidelines from human physiological, psychophysical, and neurological foundations,” *IEEE Comput. Graph. Appl.*, vol. 24, no. 2, pp. 33–39, Mar. 2004.

[94] V. G. Macefield and T. P. Knellwolf, “Functional properties of human muscle spindles,” *Journal of Neurophysiology*, vol. 120, no. 2. American Physiological Society, pp. 452–467, 01-Aug-2018.

[95] J. C. Tuthill and E. Azim, “Proprioception,” *Current Biology*, vol. 28, no. 5. Cell Press, pp. R194–R203, 05-Mar-2018.

[96] U. Proske and S. C. Gandevia, “The proprioceptive senses: Their roles in signaling body shape, body position and movement, and muscle force,” *Physiol. Rev.*, vol. 92, no. 4, pp. 1651–1697, Oct. 2012.

[97] S. Kröger, “Proprioception 2.0: novel functions for muscle spindles,” *Current opinion in neurology*, vol. 31, no. 5. NLM (Medline), pp. 592–598, 01-Oct-2018.

[98] U. Proske, “Kinesthesia: The role of muscle receptors,” *Muscle and Nerve*, vol. 34, no. 5. John Wiley & Sons, Ltd, pp. 545–558, 01-Nov-2006.

[99] P. B. C. Matthews, “Proprioceptors and their contribution to somatosensory mapping: Complex messages require complex processing,” *Canadian Journal of Physiology and Pharmacology*, vol. 66, no. 4. Can J Physiol Pharmacol, pp. 430–438, 1988.

[100] U. Proske, D. L. Morgan, and J. E. Gregory, “Thixotropy in skeletal muscle and in muscle spindles: a review,” *Prog. Neurobiol.*, vol. 41, no. 6, pp. 705–721, 1993.

[101] J. B. Fallon and V. G. Macefield, “Vibration sensitivity of human muscle spindles and Golgi tendon organs,” *Muscle \& Nerve Off. J. Am. Assoc. Electrodiagn. Med.*, vol. 36, no. 1, pp. 21–29, 2007.

[102] J. H. Anderson, “Dynamic characteristics of Golgi tendon organs,” *Brain Res.*, vol. 67, no. 3, pp. 531–537, 1974.

[103] P. Davies, J. Petit, and J. J. A. Scott, “The dynamic response of Golgi tendon organs to tetanic contraction of in-series motor units,” *Brain Res.*, vol. 690, no. 1, pp. 82–91, 1995.

[104] G. M. Goodwin, D. I. McCloskey, and P. B. C. Matthews, “The contribution of muscle afferents to keslesthesia shown by vibration induced illusionsof movement and by the effects of paralysing joint afferents,” *Brain*, vol. 95, no. 4, pp. 705–748, 1972.

[105] E. Ribot-Ciscar and J.-P. Roll, “Ago-antagonist muscle spindle inputs contribute together to joint movement coding in man,” *Brain Res.*, vol. 791, no. 1–2, pp. 167–176, 1998.

[106] A. Macerollo *et al.*, “High-frequency peripheral vibration decreases completion time on a number of motor tasks,” *Eur. J. Neurosci.*, 2018.

[107] G. Courtine, A. M. De Nunzio, M. Schmid, M. V. Beretta, and M. Schieppati, “Stance- and locomotion-dependent processing of vibration-induced proprioceptive inflow from multiple muscles in humans,” *J. Neurophysiol.*, 2007.

[108] S. M. Verschueren, S. P. Swinnen, K. Desloovere, and J. Duysens, “Effects of tendon vibration on the spatiotemporal characteristics of human locomotion,” *Exp. Brain Res.*, vol. 143, no. 2, pp. 231–239, 2002.

[109] Y. P. Ivanenko, R. Grasso, and F. Lacquaniti, “Influence of leg muscle vibration on human walking,” *J. Neurophysiol.*, vol. 84, no. 4, pp. 1737–1747, 2000.

[110] Y. Mullie and C. Duclos, “Role of proprioceptive information to control balance during gait in healthy and hemiparetic individuals,” *Gait Posture*, vol. 40, no. 4, pp. 610–615, 2014.

[111] C. Duclos, C. Kemlin, D. Lazert, D. Gagnon, J. O. Dyer, and R. Forget, “Complex muscle vibration patterns to induce gait-like lower-limb movements: Proof of concept,” *J. Rehabil. Res. Dev.*, vol. 51, no. 2, pp. 245–251, 2014.

[112] D. C. Roden-Reynolds, M. H. Walker, C. R. Wasserman, and J. C. Dean, “Hip proprioceptive feedback influences the control of mediolateral stability during human walking,” *J. Neurophysiol.*, vol. 114, no. 4, pp. 2220–2229, Oct. 2015.

[113] B.-C. Chang, M. I. Khan, A. Prado, N. Yang, J. Ou, and S. K. Agrawal, “Biomechanical differences during ascent on regular stairs and on a stairmill,” *J. Biomech.*, 2020.

[114] A. J. Paydarfar, A. Prado, and S. K. Agrawal, “Human Activity Recognition Using Recurrent Neural Network Classifiers on Raw Signals from Insole Piezoresistors,” in *Proceedings of the IEEE RAS and EMBS International Conference on Biomedical Robotics and Biomechatronics*, 2020, vol. 2020-Novem, pp. 916–921.

[115] M. Mancini, B. R. Bloem, F. B. Horak, S. J. G. Lewis, A. Nieuwboer, and J. Nonnekes, “Clinical and methodological challenges for assessing freezing of gait: Future perspectives,” *Mov. Disord.*, vol. 34, no. 6, pp. 783–790, Jun. 2019.

[116] Z. Wang and R. Ji, “Estimate spatial-temporal parameters of human gait using inertial sensors,” in *2015 IEEE International Conference on Cyber Technology in Automation, Control and Intelligent Systems, IEEE-CYBER 2015*, 2015, pp. 1883–1888.

[117] S. Minto, D. Zanotto, E. M. Boggs, G. Rosati, and S. K. Agrawal, “Validation of a Footwear-Based Gait Analysis System With Action-Related Feedback,” *IEEE Trans. Neural Syst. Rehabil. Eng.*, vol. 24, no. 9, pp. 971–980, Sep. 2016.

[118] D. Kiernan, R. O’Sullivan, A. Malone, T. O’Brien, and C. K. Simms, “Pathological Movements of the Pelvis and Trunk During Gait in Children With Cerebral Palsy: A Cross-Sectional Study With 3-Dimensional Kinematics and Lower Lumbar Spinal Loading,” *Annu. Rev. CyberTherapy Telemed.*, vol. 11, no. 2, p. 63, 2013.

[119] N. Michalopoulos, G. E. Raptis, C. Katsini, T. Chrysikos, M. Mamalakis, and A. Vigotsky, “A personalised monitoring and recommendation framework for kinetic dysfunctions: The trendelenburg gait,” *ACM Int. Conf. Proceeding Ser.*, 2016.